ARL-TR-9926 ● June 2024

A Hybrid Experimental-Modeling-Computational Framework for UHMWPE Based on Deformation and Failure Mechanisms: Extension to Off-Axis Shear Loading of Fiber-Based Composites

by Stephen L Alexander and Tusit Weerasooriya

ARL-TR-9926 ● JUNE 2024

A Hybrid Experimental-Modeling-Computational Framework for UHMWPE Based on Deformation and Failure Mechanisms: Extension to Off-Axis Shear Loading of Fiber-Based Composites

Stephen L Alexander
SURVICE Engineering Company

Tusit Weerasooriya
DEVCOM Army Research Laboratory

REPORT DOCUMENTATION PAGE

1. REPORT DATE	2. REPORT TYPE	3. DATES COVERED START DATE	END DATE
June 2024	Technical Report	27 April 2023	31 May 2024

4. TITLE AND SUBTITLE
A Hybrid Experimental-Modeling-Computational Framework for UHMWPE Based on Deformation and Failure Mechanisms: Extension to Off-Axis Shear Loading of Fiber-Based Composites

5a. CONTRACT NUMBER	5b. GRANT NUMBER	5c. PROGRAM ELEMENT NUMBER
W15P7T-19-D-0126		
5d. PROJECT NUMBER	**5e. TASK NUMBER**	**5f. WORK UNIT NUMBER**

6. AUTHOR(S)
Stephen L Alexander and Tusit Weerasooriya

7. PERFORMING ORGANIZATION NAME(S) AND ADDRESS(ES)	8. PERFORMING ORGANIZATION REPORT NUMBER
DEVCOM Army Research Laboratory ATTN: FCDD-RLA-TB Aberdeen Proving Ground, MD 21005	ARL-TR-9926

9. SPONSORING/MONITORING AGENCY NAME(S) AND ADDRESS(ES)	10. SPONSOR/MONITOR'S ACRONYM(S)	11. SPONSOR/MONITOR'S REPORT NUMBER(S)

12. DISTRIBUTION/AVAILABILITY STATEMENT
DISTRIBUTION STATEMENT A. Approved for public release: distribution unlimited.

13. SUPPLEMENTARY NOTES
ORCID: Tusit Weerasooriya, 0000-0003-3299-2166

14. ABSTRACT
We previously developed a framework for finite element simulation of UHMWPE composites at the sub-mesoscale (SMS) to interrogate deformation and failure mechanisms. The concept was applied to simulate a recent set of experiments specifically designed to address the existing knowledge gap on shear failure for these materials. These experiments characterized the shear response across loading rates of both newer film-based and more traditional fiber-based composites. We previously focused on the film-based composites and identified material parameters by matching the experimental response at each rate. Parameters were transitioned from the SMS model to a macroscale model for use in larger simulations. Here, an analogous path was followed to identify and transition material parameters for the fiber-based composites. The framework was extended to accommodate the differences between fiber-based and film-based composites. This included implementing a user defined tiebreak (UTB) model to simulate delamination with a custom-shaped traction-separation law (TSL). The high-rate material parameters that were transitioned to the macroscale model and further optimized can be used by other researchers to represent shear delamination failure of fiber-based composites under dynamic loading. Additionally, the UTB method developed here can be used for simulating delamination in other materials that may also require custom-shaped TSLs.

15. SUBJECT TERMS
ultra-high-molecular-weight polyethylene, UHMWPE, SK76 fiber, Dyneema, HB25, HB26, Tensylon, crystal plasticity, finite element simulation, Mode 2 delamination, traction-separation, interlaminar shear, LS-DYNA, slip systems, user defined tiebreak model, unidirectional ply, solid state extrusion, UHMWPE films, Sciences of Extreme Materials, Terminal Effects

16. SECURITY CLASSIFICATION OF: a. REPORT	b. ABSTRACT	C. THIS PAGE	17. LIMITATION OF ABSTRACT	18. NUMBER OF PAGES
UNCLASSIFIED	UNCLASSIFIED	UNCLASSIFIED	UU	77

19a. NAME OF RESPONSIBLE PERSON	19b. PHONE NUMBER *(Include area code)*
Tusit Weerasooriya	(410) 652-9450

STANDARD FORM 298 (REV. 5/2020)
Prescribed by ANSI Std. Z39.18

Contents

List of Figures v

List of Tables viii

Acknowledgments ix

1. Introduction 1

2. OALS Experiments 3

3. FE Simulations 6

3.1 Coordinate System for Plane Strain 6

3.2 FE Meshes 6

3.3 Boundary and Loading Conditions 7

3.4 Material Models 8

3.5 Delamination between UD Layers 9

3.5.1 Algorithm for Positive Values of Displacement at t2 10

3.5.2 Negative Values of Displacement at $t2i$ 12

3.5.3 Implementation of the UTB to Simulate Delamination 12

3.6 Overview of FE Parameter Identification 12

4. Results 13

4.1 Parameter Identification with SMS Material Model 15

4.2 Transition from Smaller Length Scale (SMS) to Larger Length Scale (EMS) Material Models 18

5. Discussion 20

5.1 Comparison of Numerical and Experimental Response 20

5.2 Shape of the TSLs 22

5.3 Rate Dependence of Simulation Parameters 22

5.4 Contributions from Each Slip System 24

5.5 Limitations 25

6. Conclusions and Transitional Outcomes 26

6.1 Summary of Findings 26

6.2 Transitional Outcomes 26

7. References 28

Appendix A. Repository of Examples Captured from Optimization Process Demonstrating the Effect of the Customized Shape of the Traction-Separation Law (TSL) on the Load-Displacement Response 30

A.1 Examples Showing How Load-Displacement Response Changes with TSL 31

A.2 Examples of Changes in TSL Shape that did not Substantially Affect the Load-Displacement Response 36

Appendix B. Effect of the Poisson's Ratios and the Out-of-Plane Shear Modulus 39

Appendix C. Collection of Examples from Preliminary Simulations Using Prebuilt Options in LS-DYNA for Triangular and Trapezoidal Traction-Separation Laws (TSLs) 42

Appendix D. How to Set Up LS-DYNA Input File to Use the User-defined Tiebreak (UTB) Model with Custom-shaped Traction-Separation Law (TSL) 46

Appendix E. How to Set Up LS-DYNA Input File to use the Sub-Mesoscale (SMS) Material Model 51

Appendix F. How to Set Up LS-DYNA to Use the Elemental Macroscale (EMS) Material Model 58

List of Symbols, Abbreviations, and Acronyms 65

List of Figures

Fig. 1 Representation of an OALS specimen, illustrating relative position within the consolidated panel prior to extraction (left) and loading configuration after extraction (right). Reproduced from Alexander et al. (2023a). 4

Fig. 2 Experimental response of HB25 composites at 15° off-axis shear loading compiled from Gunnarsson et al. (2023). Reader is referred to original report for details of the experiments. (a) Loading response with contours of maximum shear strain. Black dots indicate the yielding points selected for plotting in (b) as a function of strain rate. (b) Log plots of the yield stress and stiffness as a function of loading rate.......... 5

Fig. 3 Examples of the 15-Layer and Full-Scale FE meshes. Examples provided are from the LR simulations. The two mesh types had the same total thickness (z-direction) and width (x-direction). The thickness and width of the meshes were scaled for the specimen at each loading rate matching the corresponding experiment (Table 1). The length (out-of-plane, y-direction) of both mesh types consisted of a single element. The length was not scaled for each loading rate; for all rates, the length was 0.20 mm in the 15-Layer meshes and 0.01 mm in the Full-Scale meshes. Loading conditions are illustrated on the 15-Layer mesh, and were identical for the Full-Scale mesh. For both meshes, 14 interfaces between UD layers were modeled with tiebreak contacts (see Section 3.5); the locations of these interfaces are indicated with green arrows. 7

Fig. 4 The six slip systems assumed for a fiber-based 0° UD layer. For each slip system, only a single slip plane is shown for illustrative purposes.9

Fig. 5 Example shape of the user-defined TSL. The user inputs the slope of the initial loading regime, k, and the peak stress, SFS. The post-peak response consists of a series of line segments. In this example produced only for illustrative purposes, the post-peak response consists of three-line segments. In actual use, the user defines this response by inputting the coordinates for each of the points that are later joined by line segments.......... 11

Fig. 6 Overview of the process for determining experimentally based optimized material parameters at lower-length-scale (SMS) and macro-length-scale (EMS) modeling concepts. In all four sets of simulations, the total number of tiebreak interfaces was 14. In corresponding experiments, Mode 2 delamination failure predominantly localized into one or two interface planes (see Fig. 2a), based on dominant defects in these planes, which we were unable to identify before the experiment. 13

Fig. 7 Comparison of experimental and numerical response at each loading rate including results from Set A (labeled as "SMS, 15 Layer"), Set B

("SMS, Full-Scale"), Set C ("EMS, original"), and Set D ("EMS, optimized"). Figure 6 also explains the outcomes and purpose from each type of simulation. Contours are maximum shear strain. Note experimental and simulation scales are different but simulation scales are the same for each rate.. 14

Fig. 8 Traction–separation relationships for each rate. Left: TSLs identified using the SMS model in Set A and subsequently also used in Sets B and C. The peak traction (SFS), slope of the initial linear response (*k*), and total area under the curve (GIIC) are listed in Table 3. Right: TSLs that were re-optimized in Set D using the EMS model and iterating to match the predicted load-displacement response with the experimentally measured response. The SFS, *k*, and GIIC measurements are listed in Table 5.. 18

Fig. 9 Effect of the number of tiebreak interfaces on the simulated load-displacement response 21

Fig. 10 Log–log plots of the FE simulation parameters identified using the SMS model (Set A) against strain rate for HB25 fiber-based composites (present study) and Tensylon film-based composites (Alexander et al. 2023a). Plots in the left column are elastic constants from the SMS material model and include the fitted power law equation where applicable. Plots in the right column are from the TSLs.. 23

Fig. 11 The cumulative shear strain increment (Eq. 7) from each slip system during the Set B simulation at IR. Data collected from representative elements near center of specimen. 25

Fig. C-1 Effect of using triangular TSLs and maintaining the peak stress (SFS) and stiffness (k) constant while systematically increasing the total area under the curve (GIIC or shown in figure legend as "G2C") 43

Fig. D-1 The two curves used to define the TSLs. The first curve (LCID = 2) defines the TSL in the shear direction. The second curve (LCID = 3) defines the TSL in the normal direction. For each direction, the TSL is defined as a series of data points. The abscissa (under the A1 column) corresponds to the separation in mm, and the ordinate (under the O1 column) refers to the traction in MPa. The TSL is assumed to be formed by joining the data points with line segments. We set the TSL in the normal direction to an artificially high shape to essentially turn off delamination in the normal direction. For the shear direction, the data points listed under A1 and O1 refer to the coordinates defining the high-rate TSL reproduced in the top subfigure. All other parameters in these keywords have default values, and the reader is referred to LS-DYNA documentation for further explanation.................................. 48

Fig. D-2 The two contact keywords. Only the parameters that are highlighted in yellow have values different than the default LS-DYNA values. The highlighted non-default parameters are explained in Section D-1. The reader is referred to LS-DYNA documentation for explanation of all other parameters... 49

Fig. E-1 The material keywords for a 0° layer (top) and 90° layer (bottom). First two data cards (lines) are flags used by LS-DYNA and are described in Section E.2.1. The remaining data cards are for P1-P22, which are the material properties used in the SMS model and are described in Section E.2.2. We chose to provide the data for many of the fields via variables. The variables are included in the data cards here by prepending with the ampersand (&) symbol (e.g., the variable TAU_Y is written for P14 as "&TAU_Y"). Figure E-2 shows how to specify the variables in the input deck with the high-rate values. 53

Fig. E-2 The two keywords that define the variables used by the material keyword in Fig. E-1 with the values from the high-rate Set A values. Here, all variable names are prepended with the letter "R" (e.g., the variable TAU_Y is listed as "RTAU_Y"). 54

Fig. F-1 The material keyword. Any entry prepended with the ampersand (&) symbol (e.g., &RHO) is a variable that must be defined using the parameter keywords shown in Fig. F-2... 60

Fig. F-2 The two keywords that define the variables used by the material keyword in Fig. F-1 with the values from the high-rate Set D (re-optimized) values. Here, all variable names are prepended with the letter "R" (e.g., the variable RHO is listed as RRHO)....................... 60

Fig. F-3 Example of how to calculate the M0 and NORM0 vectors, which define the plane of the UHMWPE in the EMS model in the initial configuration. This example assumes that the UHMWPE plane is rotated only about the global 2-direction. User will need to modify for other configurations. 64

List of Tables

Table 1 Dimensions and loading rates of the HB25 specimens that were simulated from the OALS experiments 4

Table 2 Loading rates.. 8

Table 3 Parameters for Set A simulations (HB25 fiber-based composites optimized using SMS material model and 15-Layer mesh)................ 17

Table 4 EMS material model parameters used in Set C to simulate HB25 fiber-based composites based on values transitioned from SMS model 19

Table 5 EMS re-optimized values used in Set D simulations, showing changes made to the Set A optimized values.. 19

Table E-1 Material parameters used by the material keyword for running the SMS model for a 0° layer (when fibers are oriented in the global 1-direction).. 56

Table E-2 Material parameters used by the material keyword for running the SMS model for a 90° layer (when fibers are oriented in the global 2-direction).. 57

Table F-1 Material parameters used by the material keyword for running the EMS material model by means of the wrapper.................................. 63

Acknowledgments

We gratefully acknowledge the technical assistance of Richard Becker for his help with the Finite Element Computational aspect. We consulted with him for advice on computational issues throughout the course of this project. Without his guidance, it could have taken many more months for us to finish this work. Also, we greatly appreciate his thorough in-depth technical review, which greatly enhanced the content of the report.

We also acknowledge the help of David Pratt, a senior software developer at the DOD High Performance Computing (HPC) Data Analysis and Assessment Center. We often consulted his expertise in interacting with the HPC environment. His advice and code fragments have made our workflow for iteratively running and analyzing the finite element simulations on the HPC systems incomparably more efficient.

1. Introduction

Film- or fiber-based ultra-high-molecular-weight polyethylene (UHMWPE) composites are commonly formed from commercially available precursor sheets. These sheets consist of a small number of layers (typically, two to four) that have been pre-consolidated by the manufacturer. The layers are described as unidirectional (UD) because the UHMWPE films or fibers are preferentially aligned within each layer. The consumer then stacks precursor sheets according to need and preference. The stack is consolidated at elevated temperature and pressure to form the composite.

Typically, precursor fiber-based sheets have consisted of UHMWPE fibers embedded in a softer matrix, with the long axis of the fibers aligned in the orientation of the UD layer. More recently, precursor sheets have been formed by solid state extrusion (SSE) without the use fibers. These SSE sheets are referred to as films or tapes.

The fundamental difference between fiber-based and film-based composites has been shown to lead to differences in performance (Freitas et al. 2014; Cline and Love 2020; Reddy et al. 2020). However, optimizing performance requires accurate prediction of the deformation and failure response of these composites, which remains a challenge (Hoppel et al. 2021).

Finite element (FE) simulation efforts have approached this challenge at two different length scales. Subscale models attempt to separately describe each UD layer or even constituents within the layer. Therefore, each UD layer in such models is represented by one or more elements. Conversely, macroscale models describe the homogenized effect of multiple UD layers, such that each element represents multiple UD layers. As described in Liu et al. (2019), each of these two approaches has unique benefits and limitations. For example, deformation and failure mechanisms can be more directly modeled in the subscale approach. Mechanism-based modeling makes the parameters of subscale models physically based, directly linking model parameters with measurable material properties, and therefore also to processing of the laminates. For example, Liu et al. (2019) used a subscale method to investigate the effect of slip shear strength between fibers on the initiation of failure within a fiber-based composite and identified a critical shear strength that optimized performance. On the other hand, the computational expense of modeling each individual UD layer can render the subscale approach impractical in large simulations that involve multiple interacting systems in which UHMWPE is only one constituent.

One reason that accurate prediction of the response of these composites remains a challenge is due to a lack of fundamental understanding, especially regarding the newer materials and the effects of loading rate. Gunnarsson et al. (2023) recently completed a set of experiments specifically designed to address existing knowledge gaps. Loading was applied at various oblique angles relative to the axis of the UD layers to preferentially induce shear. These off-axis loaded shear (OALS) experiments were performed across strain rates from quasi-static to dynamic. Experiments were performed on a newer film-based composite as well as with a traditional fiber-based composite for comparison. The film-based composite was formed from Tensylon HSBD-30A, which is a precursor commercially available from DuPont and is hereafter referred to as Tensylon. The fiber-based composite was formed from Dyneema HB25, which consists of two UD layers in a 0°/90° layup. Dyneema HB25 differs from the more common HB26 in that the latter consists of four UD layers in a 0°/90°/0°/90° layup. In both HB25 and HB26, the UD layers contain UHMWPE fibers embedded in a polyurethane matrix. The specific UHMWPE fibers in these materials have the manufacturer designation SK76. Individual SK76 fibers have been previously mechanically characterized by Sanborn et al. (2015).

In Alexander et al. (2023a), we aimed to transition the findings of the OALS experiments on the Tensylon composites for use in the broader research community, which has been needing data on this novel material. We developed a computational framework at the sub-mesoscale (SMS) for mechanism-based FE simulation of UHMWPE composites. Each UD layer was modeled as transversely isotropic elastic with plastic slip described using a methodology adapted from crystal plasticity in metals. Slip was constrained to occur along specific slip planes based on the physical characteristics of the films. Delamination between UD layers was described with triangular traction-separation laws (TSLs): one TSL for the normal direction (Mode 1) and another for the tangential/shear direction (Mode 2). The FE parameters were optimized to match the response of the Tensylon.

Then, we transitioned the Tensylon parameters from the SMS model to a macroscale UHMWPE model that was originally developed by Becker (2019). It represents each element as consisting of multiple UD layers and was therefore referred to as elemental macroscale (EMS). We demonstrated that the EMS model with the transitioned parameters was able to match the experimental loading response of the Tensylon. Therefore, we recommended that this combination of the EMS model with the parameters we identified could be used by other researchers in larger simulations that include Tensylon but do not explicitly model each UD layer. To help aid the adoption of this method, we also documented a guide with technical details on implementing the model (Alexander et al. 2023b).

Here, the capabilities of our computational framework were extended for fiber-based composites by simulating the HB25 experiments from Gunnarsson et al. (2023). Similar to our work with Tensylon, we first identified parameters with the more detailed SMS material model. These parameters were then transitioned to the larger-scale EMS model and optimized to match the experimental response.

This report overviews the OALS experiments on HB25 composites. The details of the SMS and EMS simulations are then presented, focusing on those components that differed from the previous Tensylon simulations. The primary differences were the use of additional slip systems (altogether six slip systems) that are applicable to fiber-based systems compared to the film-based systems (four slip systems), and the implementation of a capability for using a TSL with our own custom-defined shape. The simulations are then compared to the experiments in terms of the load-displacement response and deformed shape after loading.

2. OALS Experiments

The OALS experiments have been fully documented by Gunnarsson et al. (2023), and the reader is referred to original documentation for complete details. This report focuses on the fiber-based composites formed from the commercially available Dyneema HB25 precursors. These precursors consist of two UD layers pre-consolidated in orthogonal directions (0°/90°).

A total of 189 precursor sheets (378 UD layers) were stacked and then consolidated to form a panel. Figure 1 (left) shows a schematic representation of the consolidated panel and subsequent extraction of individual specimens. A waterjet cutter was used to extract specimens at different angles, θ, from the axis of the UD layers. The experiments used here for obtaining FE parameters were performed at θ = 15° low angle to avoid the effect of normal splitting as that is observed at high angles. Figure 1 also shows the loading configuration. Loading was applied at three different rates: low-rate (LR), intermediate-rate (IR), and high-rate (HR). One typical representative experiment was simulated at each rate.* Table 1 provides the dimensions and loading rates for the three simulated specimens.

Figure 2 shows the loading response measured in the experiments. The experiments measured the loading response of the specimens at the far-field, quantifying the overall response of the composite materials. The yield strength and stiffness of the composites measured in the experiments were highly sensitive to strain rate.

* In the Gunnarsson et al. (2023) report that documents the OALS experiments, specimens are referred to using a three-part syntax for ease of identification. The specimens simulated here at LR, IR, and HR were referred to as HB25-15DEG-C03, HB25-15DEG-C04, and HB25-15DEG-C01, respectively.

Dyneema SK76 UHMWPE fibers, which are the constituent fibers in the HB25 composites, showed minimal rate sensitivity for the fiber longitudinal modulus per measurements by Sanborn et al. (2015). Therefore, the rate sensitivity observed here could be due to the strain sensitivity of slipping between fibers. The goal of the iterative FE simulations of the present report was to determine responses of the component materials within the composite so as to reproduce the far-field responses shown in Fig. 2.

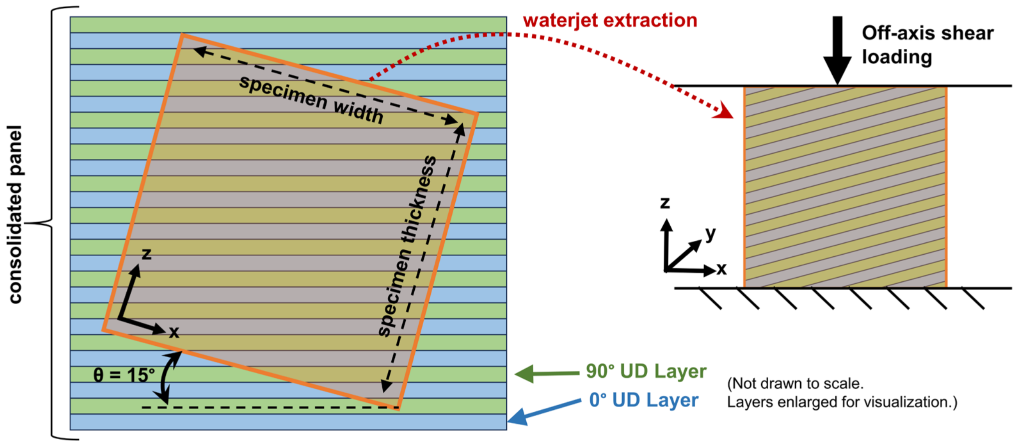

Fig. 1 Representation of an OALS specimen, illustrating relative position within the consolidated panel prior to extraction (left) and loading configuration after extraction (right). Reproduced from Alexander et al. (2023a).

Table 1 Dimensions and loading rates of the HB25 specimens that were simulated from the OALS experiments

Loading rate	Thickness in z-direction (mm)	Width in x-direction (mm)	Length in y-direction (mm)	Experimental loading rate (m/s)	Experimental strain rate (1/s)
LR	9.37	10.10	10.11	5×10^{-6}	5×10^{-4}
IR	9.16	10.02	10.05	5×10^{-3}	5×10^{-1}
HR	7.59	10.21	9.93	5.53	7×10^{2}

Note: Figure 1 shows x–y–z coordinate system.

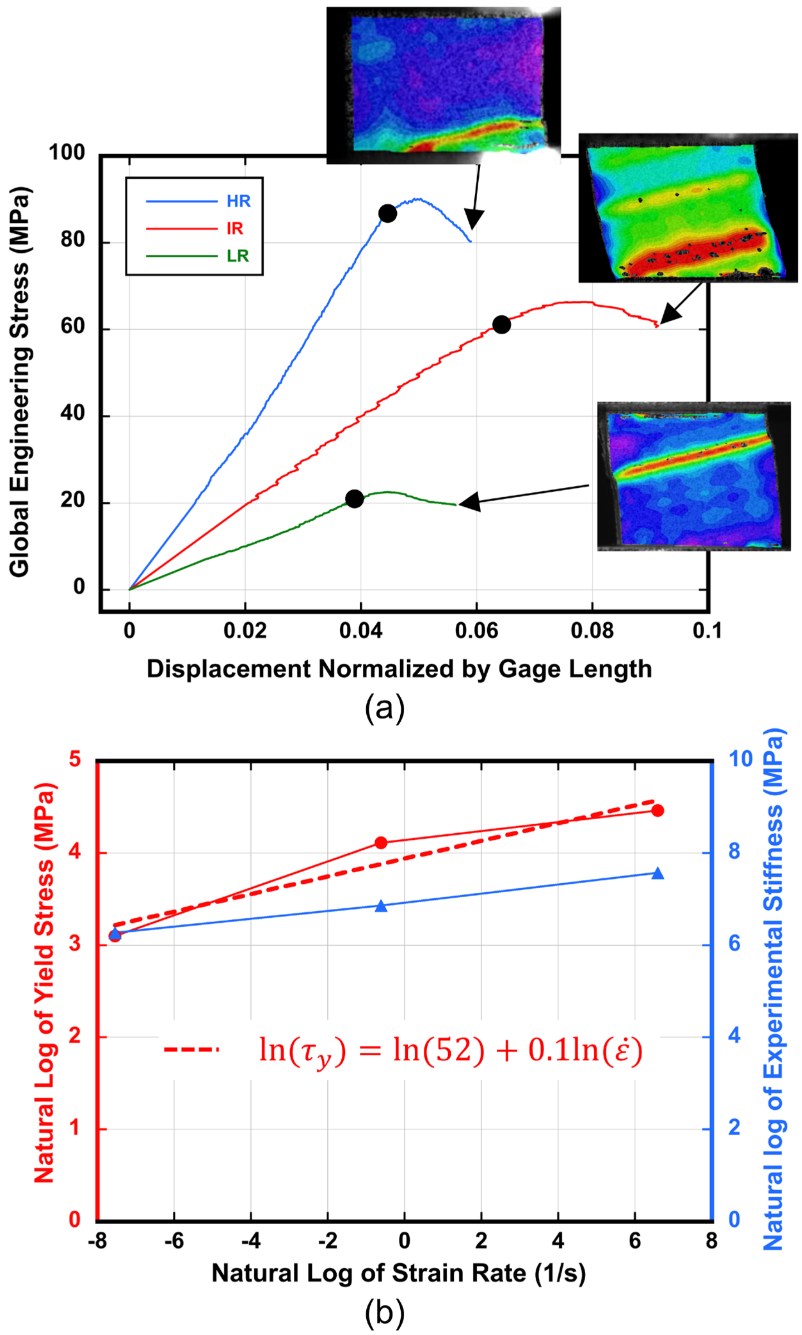

Fig. 2 Experimental response of HB25 composites at 15° off-axis shear loading compiled from Gunnarsson et al. (2023). Reader is referred to original report for details of the experiments. (a) Loading response with contours of maximum shear strain. Black dots indicate the yielding points selected for plotting in (b) as a function of strain rate. (b) Log plots of the yield stress and stiffness as a function of loading rate.

3. FE Simulations

Explicit FE simulations were carried out with a developmental version of the LS-DYNA (ANSYS 2023) solver on DOD High Performance Computing machines. Material models, FE meshes, and boundary conditions were analogous to the Tensylon simulations in most of the details reported by Alexander et al. (2023a). Therefore, only those points where the present fiber-based simulations were fundamentally different than the Tensylon simulations are fully described here. Only a brief overview is provided for the remaining details. Reader is referred to the previous report for a full description.

3.1 Coordinate System for Plane Strain

The experiments were simulated under the assumption of plane strain. The coordinate system was defined such that compressive loading was applied in the z-direction, as shown in Fig. 1. Deformation was constrained in the out-of-plane direction (y-direction).

3.2 FE Meshes

Two FE meshes were used for each loading rate. All meshes used the LS-DYNA default element type, which is a constant stress hexahedral element. The difference between the two meshes at each loading rate was in mesh refinement. Figure 3 shows the two meshes used in the LR simulations as an example.

The total thickness (z-dimension, Fig. 3) of the specimen was the same for both mesh types and was specified to match the experiment (Table 1). The coarser mesh divided the specimen thickness into 15 UD layers. These "15-Layer" meshes consisted of a total of 2,176 elements. The thickness of each of the 15 UD layers was nominally spanned by 4 elements. There were 14 interfaces between the UD layers, which are numbered in Fig. 3 (left). The nodes at these interfaces were not merged. Contact at each of the interfaces was simulated using the tiebreak model described in Section 3.5.

The more refined "Full-Scale" mesh divided the specimen thickness into 206 UD layers. There were 205 total interfaces between the layers. Only 14 of these interfaces were modeled with tiebreak contacts (Section 3.5). These 14 tiebreak interfaces are identified in Fig. 3 (right). The nodes across the remaining 191 interfaces were merged. The 14 interfaces modeled with tiebreak contacts were chosen to approximately match the location of the 14 interfaces in the 15-Layer mesh, which can be seen by comparing the positions of the contact interfaces between the two mesh types in Fig. 3 (green arrows). In the Full-Scale mesh the thickness of each UD layer was nominally spanned by 6 elements, with 587,868 total elements.

All meshes consisted of only a single element in the y-dimension. The y-dimension length was 0.20 microns in the 15-Layer meshes and 0.01 microns in the Full-Scale meshes. The x- and z-dimensions of the 15-Layer and Full-Scale meshes were scaled using a custom Python script for each loading rate to match the dimensions of the specimen in the corresponding experiment (Table 1).

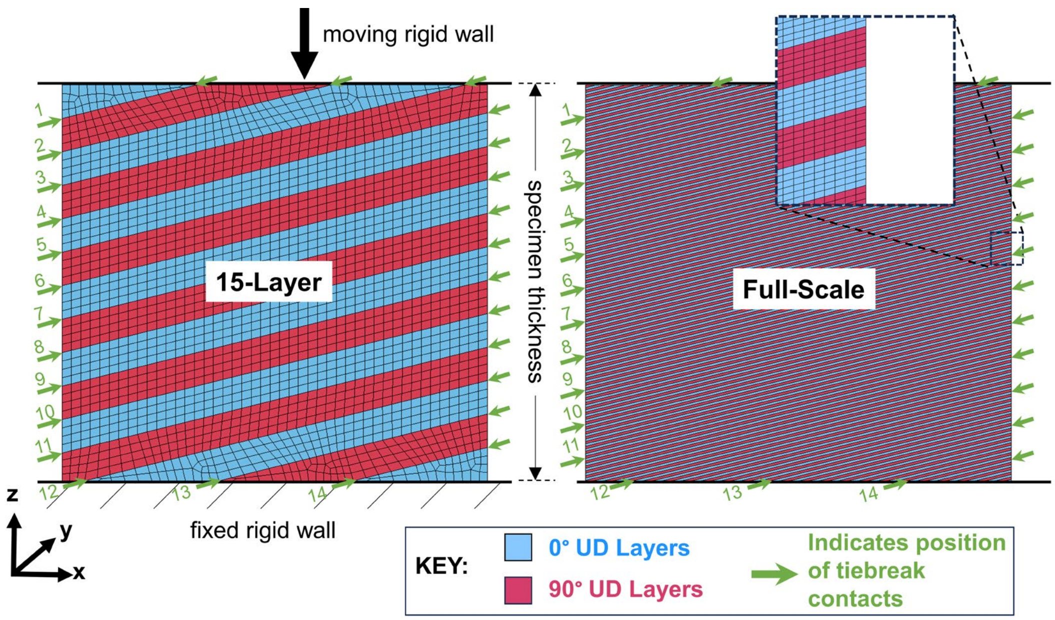

Fig. 3 Examples of the 15-Layer and Full-Scale FE meshes. Examples provided are from the LR simulations. The two mesh types had the same total thickness (z-direction) and width (x-direction). The thickness and width of the meshes were scaled for the specimen at each loading rate matching the corresponding experiment (Table 1). The length (out-of-plane, y-direction) of both mesh types consisted of a single element. The length was not scaled for each loading rate; for all rates, the length was 0.20 mm in the 15-Layer meshes and 0.01 mm in the Full-Scale meshes. Loading conditions are illustrated on the 15-Layer mesh, and were identical for the Full-Scale mesh. For both meshes, 14 interfaces between UD layers were modeled with tiebreak contacts (see Section 3.5); the locations of these interfaces are indicated with green arrows.

3.3 Boundary and Loading Conditions

As shown in Fig. 3, a stationary rigid wall was placed at the bottom of the specimen. A moving rigid wall was placed at the top of the specimen. Velocity was specified in the z-direction with magnitude shown in Table 2. A scaling factor was used to decrease computation time for the IR and LR simulations. The IR and LR scaling factors were the same values as those used in the film-based simulations; additional details describing the process for identifying these values were given in Alexander et al. (2023a). Contact between the walls and the specimen was modeled as frictionless sliding because the experiments used lubricant at the interfaces.

Table 2 Loading rates

Loading rate	Experimental loading velocity (m/s)	Simulation loading velocity (m/s)	Scaling factor
LR	5×10^{-6}	5×10^{-1}	1×10^{5}
IR	5×10^{-3}	2.0	4×10^{2}
HR	5.53	5.53	[none]

3.4 Material Models

The fiber-based simulations used either the SMS or the EMS UHMWPE material models, which have been previously documented in Alexander et al. (2023a) and Becker (2019).

For convenience, the plastic slip relations of the SMS and EMS models for each slip system, α, are reproduced in Eqs. 1 and 2, respectively. Reader is referred to Alexander et al. (2023a) for explanations regarding the parameters of these equations and for the remaining details of the SMS and EMS material models. Briefly, we recall here that the SMS approach was at the length-scale of a single UD layer. The UD layer was modeled as transversely isotropic elastic. The preferred direction was referred to as the "fiber" or "film" direction, the f-direction. The two transverse directions, t-directions, formed the plane of isotropy. A 0° UD layer was defined by having the f-direction aligned in the 1-direction. A 90° UD layer was defined by having the f-direction aligned in the 2-direction.

Due to transverse isotropy, the SMS model had five independent elastic constants: two Young's moduli (E_f and E_t), two Poisson's ratios (ν_{tt} and ν_{ft}), and one shear modulus (G_{ft}). The shear modulus describing shearing within the transverse plane, G_{tt}, was not independent due to the assumption of transverse isotropy, but was described by Eq. 3. The parameters for the material models were identified through iterative simulations as described in Section 3.6.

$$\dot{\gamma}_n^\alpha = \dot{\gamma}_0 \left(\frac{\tau_n^\alpha}{\tau_y^0}\right)^{\frac{1}{m}} sgn[\tau_n^\alpha], \quad (1)$$

$$\tau^\alpha = \hat{\tau}_0 \left(1 + \hat{c}\,\frac{\dot{\gamma}^\alpha}{\hat{\dot{\gamma}}_0}\right)^{\widehat{m}} \quad (2)$$

$$G_{tt} = \frac{E_t}{2(1+\nu_{tt})} \quad (3)$$

The only difference with the previously documented film-based models was in the number of slip systems assumed in the SMS model. The previous film-based simulations assumed four total slip systems based on the structure of the films. Here, the UHMWPE fibers within each UD layer were approximated as close packed. This assumption accommodated six slip systems. The six slip systems are illustrated in Fig. 4 for a 0° UD layer. Slip systems $\alpha = 1$ and $\alpha = 2$ are two instances of pencil glide along the fiber direction with different, orthogonal slip planes. Slip direction could have been associated with other planes in addition to the two orthogonal planes. However, slip in these additional planes are restricted by the adjacent 90° rotated layers due to the 0°/90° arrangement of the layers in the layup of the composite.

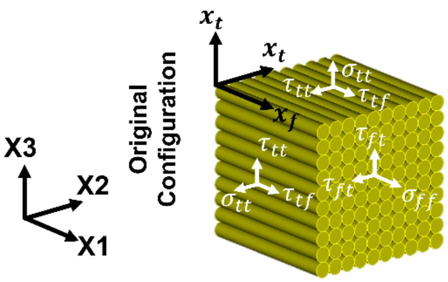

Slip System (α)	Slip Direction ($s^{\alpha,0}$)	Slip Plane Normal ($m^{\alpha,0}$)
1	(1,0,0)	(0,1,0)
2	(1,0,0)	(0,0,1)
3	(0,1,0)	(0,0,1)
4	(0,0,1)	(0,1,0)
5	(0,1/√2, 1/√2)	(0,-1/√2, 1/√2)
6	(0,-1/√2, 1/√2)	(0,-1/√2, -1/√2)

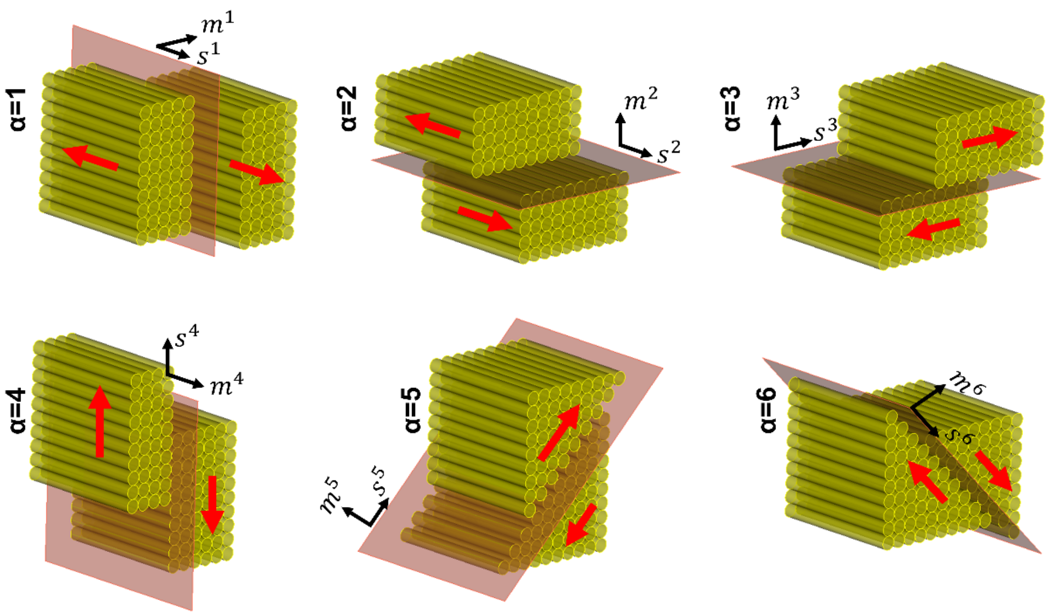

Fig. 4 The six slip systems assumed for a fiber-based 0° UD layer. For each slip system, only a single slip plane is shown for illustrative purposes.

3.5 Delamination between UD Layers

Delamination between the 14 specific UD layers identified in Fig. 3 was simulated using the tiebreak contact formulation of LS-DYNA with a user-defined tiebreak (UTB) model. LS-DYNA called the UTB for each *i*-th timestep during the FE simulation, which spanned from t_1^i to t_2^i. At each timestep, and for each contact pair, LS-DYNA supplied the UTB with the separation distance (or displacement, δ) at the time t_2^i in both the normal direction ($\delta_n^{t_2^i}$) and tangential/shear direction ($\delta_s^{t_2^i}$). The UTB then calculated the corresponding traction at t_2^i for the normal direction ($\sigma_n^{t_2^i}$) and shear direction ($\sigma_s^{t_2^i}$).

We developed the UTB to enable one TSL to be defined for the normal direction (Mode 1) and an additional, independent TSL to be defined for the tangential/shear direction (Mode 2). The algorithm for calculating traction from the TSL was analogous between the two modes for positive values of $\delta_n^{t_2^i}$ and $\delta_s^{t_2^i}$. The algorithms only differed between the two modes for negative values of displacement. Therefore, the UTB framework is first presented here for the case of positive values of displacement. Next, the case for negative values of displacement is discussed. Finally, additional details are presented regarding the implementation of the UTB in the fiber-based OALS simulations.

3.5.1 Algorithm for Positive Values of Displacement at t2

The algorithm for calculating the normal traction at t_2^i for positive values of normal displacement ($\delta_n^{t_2^i}$) was analogous to the algorithm for calculating the shear traction at t_2^i for positive values of shear displacement ($\delta_s^{t_2^i}$). Therefore, these algorithms are presented here in a generic sense applicable to both modes by referring to the current displacement value supplied by LS-DYNA (either normal or shear) as $\delta^{t_2^i}$ and the traction calculated by the algorithm (either normal or shear) as $\sigma^{t_2^i}$.

Figure 5a provides an example of the general shape of the TSL. Initial loading followed a linear relation from δ = 0, σ = 0 to the peak at δ_0, SFS (Shear Failure Stress). The slope of the initial linear loading regime was referred to as k. For displacement beyond δ_0, the traction reduced to 0 along a series of line segments that were defined by the user. The displacement at which traction reached 0 was referred to as the failure displacement, δ_F. If the displacement ever reached beyond δ_F, the contact pair was considered to be completely separated and the traction was no longer calculated by the UTB.

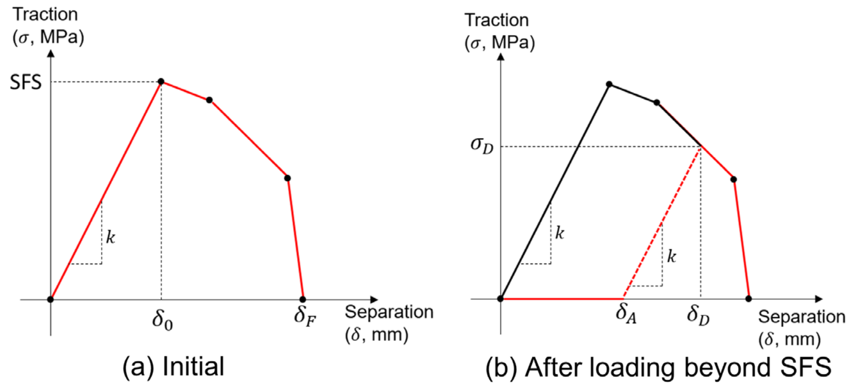

Fig. 5 Example shape of the user-defined TSL. The user inputs the slope of the initial loading regime, *k*, and the peak stress, SFS. The post-peak response consists of a series of line segments. In this example produced only for illustrative purposes, the post-peak response consists of three-line segments. In actual use, the user defines this response by inputting the coordinates for each of the points that are later joined by line segments.

The algorithm calculated the traction from the current value of $\delta^{t_2^i}$ and the user-defined shape of the TSL by two different methods depending on whether the contact pair had already been separated by a displacement greater than δ_0 in any previous timestep thus far in the simulation. The first method (Fig. 5a) was for the case when the contact pair had not yet been separated by a distance greater than δ_0, for example, at the beginning of the simulation. For this case, the traction was calculated simply by locating the corresponding point along the user-defined TSL for the given $\delta^{t_2^i}$, indicated by the red lines in Fig. 5a.

The second method was for the case when the contact pair had already been separated by a distance greater than δ_0 during a previous increment in the simulation. Figure 5b provides an example to illustrate this case. To calculate the traction, first the UTB loaded from the history variables the maximum distance that the contact pair had been previously separated during the simulation, which had been saved as a history variable, δ_D. Next, the corresponding stress on the user-defined TSL was located with coordinates δ_D, σ_D. Then, the linear unloading/re-loading relationship was determined by connecting the point at δ_D, σ_D with the $\sigma = 0$ horizontal axis by a line with the same slope, k, as the initial loading regime. The point at which this line intersected with the $\sigma = 0$ axis was identified as δ_A. Finally, the UTB determined the traction from the relative value of $\delta^{t_2^i}$ by the following conditions, which are illustrated by the red lines in Fig. 5b:

$$\sigma^{t_2^i} = \begin{cases} 0 & if\ 0 \leq \delta^{t_2^i} \leq \delta_A \\ k \cdot \left(\delta^{t_2^i} - \delta_A\right) & if\ \delta_A < \delta^{t_2^i} \leq \delta_D \\ (from\ curve) & if\ \delta_D < \delta^{t_2^i} \leq \delta_F \\ 0 & if\ \delta^{t_2^i} > \delta_f \end{cases} \tag{4}$$

3.5.2 Negative Values of Displacement at t_2^i

The UTB calculated the normal traction for the case when the displacement in the normal direction ($\delta_n^{t_2^i}$) was negative as: $\sigma_n^{t_2^i} = k \cdot \delta_n^{t_2^i}$. Thus, in compression, the UTB acted as a linear spring with the same stiffness as the initial loading in tension. For negative values of shear displacement ($\delta_s^{t_2^i}$), the UTB calculated the shear traction by first taking the absolute value of $\delta_s^{t_2^i}$ and then applying the algorithm described previously for positive values. Thus, the UTB modeled shear delamination in either direction to be equivalent.

3.5.3 Implementation of the UTB to Simulate Delamination

We assumed that the loading configuration of the OALS experiments preferentially induced Mode 2 over Mode 1 delamination. Therefore, in the present simulations, the Mode 1 TSL was set to be orders of magnitude higher than the Mode 2 TSL. All interfaces were modeled using the same shape for the Mode 2 TSL. This shape was identified through iterative simulations as described in Section 3.6.

A two-way automatic contact was also specified at each tiebreak contact with default parameters. This additional specification was included based on dialog with LS-DYNA support. It was recommended in order to reduce interpenetration in compression that could arise due to using lower values of stiffness in the UTB.

3.6 Overview of FE Parameter Identification

The FE simulations had two groups of parameters: those for the material models and those for the TSL used to model interlayer delamination. Plasticity in the SMS and EMS models was rate dependent (see Eqs. 1 and 2), so the plastic response can be represented by a single set of parameters that are applicable across strain rates. However, such functional forms relating to strain rate are not available for the transversely isotropic elastic and the tiebreak de-cohesive behavior, as far as we are aware. Therefore, the elastic and tiebreak parameters were optimized for each loading rate to represent the experimental observation. As depicted in Fig. 6, these parameters were optimized through a process involving four different sets of simulations: Sets A, B, C, and D. Each set consisted of three subsets of simulations, one at each loading rate (LR, IR, and HR), that were run with the same mesh type (either 15 [0°/90°]-UD-Layer or Full-Scale) and material model (EMS or SMS).

Figure 6 overviews the process. First, in Set A the parameters were identified using the lower length scale material model (SMS) with the 15 [0°/90°]-UD-Layer mesh type. The fewer number of elements in this mesh, compared to the Full-Scale mesh, enabled faster run times and thus allowed for quicker iterations. Next, in Set B, the parameters were checked with the Full-Scale 206 [0°/90°]-UD layer model with approximately six elemental layers/UD layer. This provided a set of rate-dependent responses at lower-length-scale to compare with the corresponding homogenized higher-length-scale responses to observe the effect of length scale and homogenization on the responses. Then, the optimized lower-length-scale parameters were transitioned to macro-length-scale of the EMS model (Set C) to compare with the effect of length-scale and homogenization on the response. Finally, the EMS parameters were re-optimized to better match the experimental load-displacement response (Set D) and to provide to other researchers. Additional information regarding the specific parameter values for the SMS and EMS model are presented in Section 4, Results.

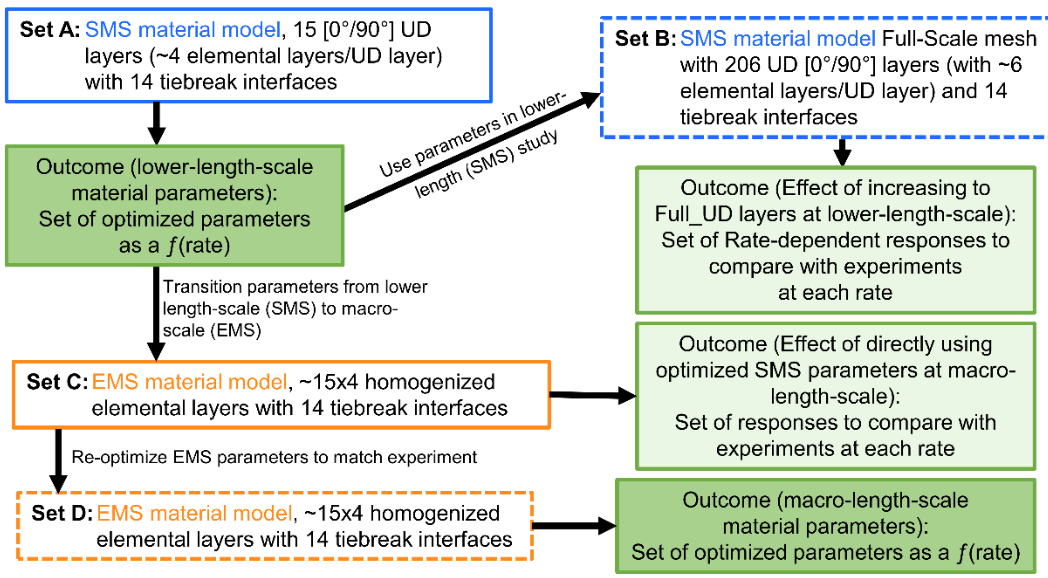

Fig. 6 Overview of the process for determining experimentally based optimized material parameters at lower-length-scale (SMS) and macro-length-scale (EMS) modeling concepts. In all four sets of simulations, the total number of tiebreak interfaces was 14. In corresponding experiments, Mode 2 delamination failure predominantly localized into one or two interface planes (see Fig. 2a), based on dominant defects in these planes, which we were unable to identify before the experiment.

4. Results

Figure 7 provides an overview comparing the numerical and experimental responses from Sets A through D. The subsequent Sections 4.1 and 4.2 provide additional information regarding the SMS simulations (Sets A and B) and EMS simulations (Sets C and D), respectively.

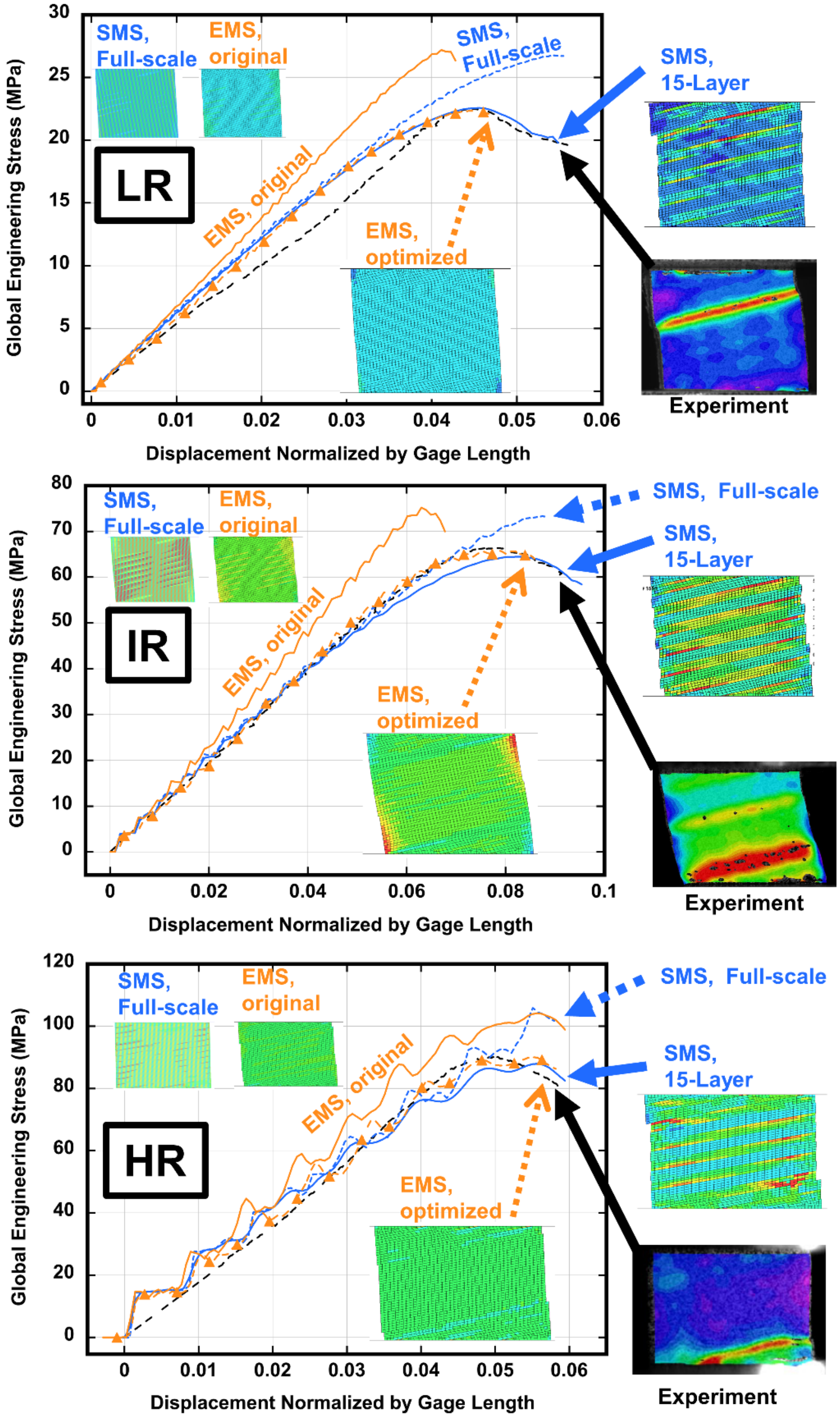

Fig. 7 Comparison of experimental and numerical response at each loading rate including results from Set A (labeled as "SMS, 15 Layer"), Set B ("SMS, Full-Scale"), Set C ("EMS, original"), and Set D ("EMS, optimized"). Figure 6 also explains the outcomes and purpose from each type of simulation. Contours are maximum shear strain. Note experimental and simulation scales are different but simulation scales are the same for each rate.

4.1 Parameter Identification with SMS Material Model

The FE parameter values were first determined with the Set A simulations, which used the SMS material model and 15-[0°/90°] UD-Layer (with ~4 elemental layers/UD layer) mesh. Table 3 lists the parameter values from Set A for the SMS material model and the tiebreak contacts. Figure 8 (left) shows the shapes of the TSL at each rate. Set B used the exact same optimized parameter values but with the Full-Scale mesh.

The SMS material model required five independent elastic constants and three parameters describing crystal plasticity (listed in Section 3.4). The tiebreak contacts required specification of the shape of the TSL. The method for identifying these parameter values was based on the general process outlined as follows. First, we assumed fixed values for five of the SMS material model parameters. The source of these non-optimized parameters is identified in the "Source" column of Table 3. Next, initial values of τ_y^0 and m were identified from the relationship between yield stress and strain rate that was found in the experiments (Fig. 2b). The initial values were then iterated by comparing the final contour shape after loading. The slope of the relationship between yield stress and strain rate in the experiments indicated a value of $m = 0.1$; however, using this value in simulations was not showing experimentally observed plastic shearing between layers before localization. But, using a value of $m = 0.15$ induced shearing within layers that is comparable with experimentally observed shearing.

Next, the linear portion of the simulated load-displacement response was iterated to be comparable with the slope of the experimentally measured initial load-displacement response by adjusting the transverse modulus E_t because this parameter governed the through-thickness compressive stiffness, as documented in Appendix C of Alexander et al. (2023a). Finally, the shape of the TSL was adjusted to match the post-peak response. Appendix A is an unstructured repository of specific examples captured during the optimization process showing the shape of TSLs and their corresponding load-displacement responses. The reader seeking further detail can see the effect of the custom-defined shape of the TSL on post-peak response by comparing these examples.

The effect on the load-displacement response of each of the parameters was qualitatively the same as in the simulations of Tensylon composites in Alexander et al. (2023a). Reader is referred to Appendix C of Alexander et al. (2023a), which provides examples of the effects of many of these parameters. Here, we provide additional details on two points. First, Appendix C of Alexander et al. (2023a) did not specifically document the effect of the Poisson's ratios and shear moduli. The SMS model had only one independent shear modulus, G_{ft}, and two independent

Poisson's ratios, ν_{ft} and ν_{tt}. Appendix B of the present report provides an example of the effect of these elastic constants. Changes in G_{ft} by orders of magnitude affected the peak stress but not the stiffness, while smaller changes did not significantly affect the load-displacement response. The Poisson's ratio ν_{ft} did not appear to have an effect. The Poisson's ratio in the transverse plane, ν_{tt}, had a noticeable effect, likely due to the inverse dependence of the in-plane shear modulus G_{tt} on ν_{tt} (Eq. 3). Thus, decreasing ν_{tt} increased G_{tt}, which noticeably affected the overall response of the off-axis-loaded shear specimen by reducing the stiffness and increasing peak stress.

In addition, the Tensylon simulations of Alexander et al. (2023a) used triangular TSLs. The shape of the triangle was defined by three parameters: the peak stress (SFS), initial slope (k), and total area under the curve (GIIC). For the present fiber-based simulations, the initial linear response was still defined by SFS and k, but the post-peak response was defined by the customized line segments by which the traction returned to zero after the peak (example schematic in Fig. 5).

Table 3 Parameters for Set A simulations (HB25 fiber-based composites optimized using SMS material model and 15-Layer mesh)

Parameter[a]	Description (units)	Values			Source
		LR	IR	HR	
SMS Material Model					
E_f	Young's modulus in primary direction of layer (MPa)	110,000	110,000	110,000	Sanborn et al. (2015)
E_t	Young's modulus in transverse direction (MPa), governing the through-thickness stiffness	500	850	1500	Optimized[b]
ν_{ft}	Poisson's ratio between primary and transverse directions	0.35	0.35	0.35	Assumed same as Tensylon
ν_{tt}	Poisson's ratio in the transverse plane	0.50	0.50	0.50	Liu et al. (2019)
G_{ft}	Out-of-plane shear modulus[c] (MPa)	3000	3000	3000	Liu et al. (2019)
$\dot{\gamma}_0$	Reference shear strain rate (s^{-1})[d]	1 [b]	1 [b]	1	Assumed
τ_y^0	Reference shear yield strength of UD layer (MPa)	18.0	18.0	18.0	Optimized[b]
m	Rate sensitivity exponent	0.15	0.15	0.15	Optimized[b]
TSL for Tiebreak Contacts[e]					
SFS	Shear failure strength, peak of TSL (MPa)	6.1	16.0	18.0	Optimized[b]
k	Slope of initial part of TSL (MPa/mm)	4000	4000	4000	Optimized[b]
GIIC	Energy release rate (MPa × mm)	7.31	9.27	17.27	Optimized[b]

[a] Reader is referred to Alexander et al. (2023a) for definitions of the parameters. A brief overview of the SMS material model parameters has also been provided in Section 3.4.
[b] Optimized by iteratively comparing the numerical output with the corresponding experimental response and adjusting parameters to reduce the error between them.
[c] Because the SMS model assumed transverse isotropy, G_{ft} was the only independent shear modulus. The in-plane shear modulus, G_{tt} was dictated by Eq. 3 (see Section 3.4). Since ν_{tt} was taken as 0.5, Eq. 3 indicates that the in-plane shear modulus was $G_{tt} = E_t/3$ for all rates.
[d] Even though the reference shear strain rate is 1, we increased it for the LR and IR simulations to speed up the calculation by multiplying the rate by the scaling factor (SF) listed in Table 2.
[e] Figure 8 (left) shows the shape of the TSLs.

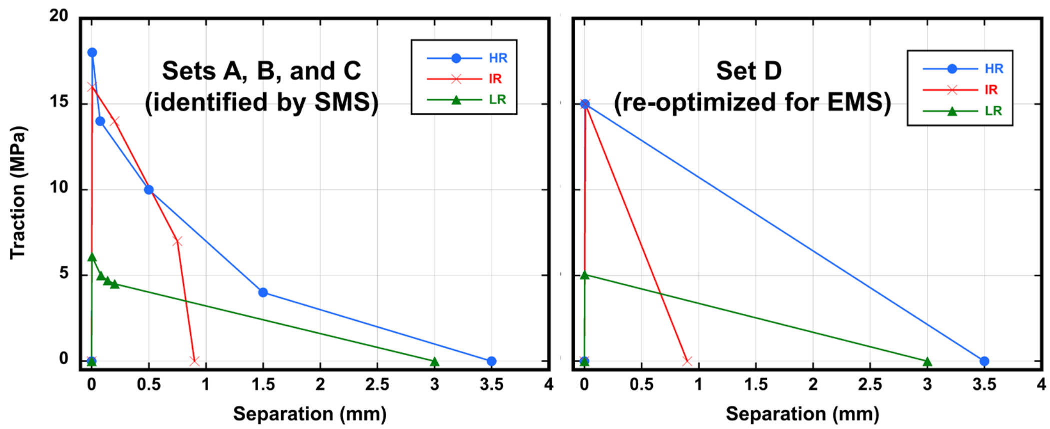

Fig. 8 Traction–separation relationships for each rate. Left: TSLs identified using the SMS model in Set A and subsequently also used in Sets B and C. The peak traction (SFS), slope of the initial linear response (*k*), and total area under the curve (GIIC) are listed in Table 3. Right: TSLs that were re-optimized in Set D using the EMS model and iterating to match the predicted load-displacement response with the experimentally measured response. The SFS, *k*, and GIIC measurements are listed in Table 5.

4.2 Transition from Smaller Length Scale (SMS) to Larger Length Scale (EMS) Material Models

The values that were identified for the SMS material model were transitioned to the EMS model (Fig. 6). The set of LR, IR, and HR simulations that used the EMS model with these transitioned values was named Set C. Table 4 lists the EMS material model parameters used in Set C and provides additional information on the transition from the SMS to EMS parameters. Set C used the same TSLs as the SMS simulations (Fig. 8, left). However, the Set C simulations were stiffer than the experiments and failed at higher peaks (see Fig. 7). Therefore, the TSLs together with two of the EMS parameters were obtained by re-optimizing the EMS parameters to represent the experimentally measured load-displacement responses. The set of simulations that used these EMS re-optimized values was named Set D. Table 5 lists these EMS re-optimized values and Fig. 8 (right) plots the resultant traction–separation relationships. Most of the updated values were identified through iterative optimization. The exception was the matrix bulk modulus, κ. The retuned values of κ were directly calculated by the same equation as in Set C (Eq. 6 in Table 4), only reducing the Poison ratio value of ν_{ft} from 0.35 to 0.30.

Table 4 EMS material model parameters used in Set C to simulate HB25 fiber-based composites based on values transitioned from SMS model

EMS model param.[a]	Description	Values			Source[b]
		LR	IR	HR	
ρ	Material density (kg/m^3)	994	994	994	Alexander and Weerasooriya (2021)
μ	Matrix shear modulus (MPa)	167	283	500	From SMS: $\frac{E_t}{2(1+\nu_{tt})}$ (5)
κ	Matrix bulk modulus (MPa)	556	944	1,667	From SMS: $\frac{E_t}{3(1-2\nu_{ft})}$ (6)
κ'	Pressure derivative of κ	8	8	8	Becker (2019)
$\hat{\tau}_0$	Matrix shear yield strength (MPa)	2.885	2.885	2.885	Based on SMS: τ_y^0, m
$\hat{c}$	Slip rate constant	2×10^5	2×10^5	2×10^5	Based on SMS: τ_y^0, m
$\hat{m}$	Strain rate exponent	0.15	0.15	0.15	From SMS: m
$\dot{\hat{\gamma}}_0$	Reference slip rate (s^{-1})[c]	1	1	1	From SMS: $\dot{\gamma}_0$
E	Fiber/film elastic modulus (MPa)	110,000	110,000	110,000	From SMS: E_f
σ_{ff}	Failure stress for single fiber/film (MPa)	4000	4000	4000	Sanborn et al. (2015)

Note: For the TSL parameters, Set C used the Set A optimized values (listed in Table 3).
[a] Reader is referred to previous documentation for definitions of these parameters (Becker 2019; Alexander et al. 2023a).
[b] Parameters in red were from the SMS material model, with values given in Table 3.
[c] Even though the reference shear strain rate is 1, we increased it for the LR and IR simulations to speed up the calculation by multiplying the rate by the SF listed in Table 2.

Table 5 EMS re-optimized values used in Set D simulations, showing changes made to the Set A optimized values

Param.	Description (units)	Values		
		LR	IR	HR
EMS Material Model				
κ	Matrix bulk modulus (MPa)	417	708	1250
$\hat{\tau}_0$	Matrix shear yield strength (MPa)	2.2	2.2	2.2
TSL for Tiebreak Contacts[a]				
SFS	Shear failure strength, peak of TSL (MPa)	5.05	15.00	15.00
k	Slope of initial part of TSL (MPa/mm)	4000 (from Set A)	2000	4000 (from Set A)
GIIC	Energy release rate (MPa × mm)	7.58	6.75	26.25

[a] Figure 8 (right) shows the shape of the TSLs.

5. Discussion

5.1 Comparison of Numerical and Experimental Response

The images from the experiments in Fig. 7 show that the specimens in the experiments deformed from their originally rectangular shape to a rhombic shape. This deformation was due to the off-axis orientation of the UD layers relative to the loading direction as shown in the schematic of Fig. 1. The rhombic shape was more exaggerated for LR and IR. At HR, the specimen was more brittle and had less deformation prior to catastrophic failure. Both the SMS and EMS material models replicated this rate-dependent change of shape, as shown in the contours in Fig. 7.

The experimental images in Fig. 7 also show a single zone of strain localization within each specimen. These areas are oriented at approximately the same off-axis angle (15°) as the off-axis angle between the UD layers and the loading direction. Therefore, the strain localization was likely at a critical interlayer interface within the specimen. The SMS material model showed several areas of interlayer strain concentrations. We can assume that the particular interface that initiated failure in the experiments was determined by dominant defects/flaws either in the raw material or arising from processing between layers, which was not captured by the simulations. The EMS material model did not have similar interlayer strain concentrations because it did not explicitly model the UD layers but instead represented the specimen as a homogeneous material.

Among all of the simulations, Set A most closely matched the load-displacement response of the experiments since the FE parameters were originally identified for this set with the SMS material model and 15-Layer mesh. In Set B, the same parameters were then applied to the Full-Scale mesh. The change in mesh type did not significantly affect the slope of the initial loading regime. However, the change in mesh type appeared to delay the onset of failure, with higher peak stress occurring at higher values of normalized displacement. This difference in failure could be due to difference between the 15-Layer and Full-Scale mesh in the amount of interlayer interfaces relative to the entire specimen. In the 15-Layer mesh, delamination was modeled at all of the 14 interlayer interfaces. Conversely, the Full-Scale mesh had a total of 205 interlayer interfaces for plastic deformation, but delamination was modeled at only 14 of them. In the remaining 191 interlayer interfaces, the nodes were fully merged. We hypothesize that increasing the number of tiebreak interfaces in the Full-Scale mesh at which delamination was modeled would decrease the peak stress in the Set B simulations. The effect of the number of tiebreak interfaces on the computed response was verified by rerunning the IR Set A simulation, which used the SMS material model with the 15-Layer mesh.

Figure 9 summarizes the findings. In the original simulation, all 14 interfaces between UD layers were modeled with tiebreak contacts. In the modified simulation, the nodes across six of the interfaces were merged such that there were only eight interfaces modeled with tiebreak contacts (indicated by green arrows in Fig. 9). The simulated responses confirm that increasing the number of tiebreak interfaces (transitioning from red to blue curves in Fig. 9) reduces the peak stress and causes the peak to occur at lower values of normalized displacement. The initial stiffness does not appear to be affected.

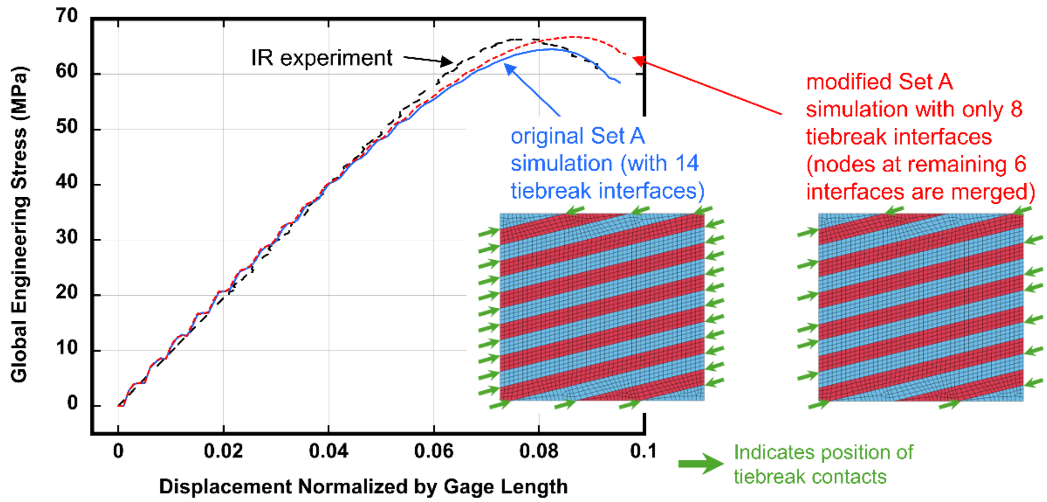

Fig. 9 Effect of the number of tiebreak interfaces on the simulated load-displacement response

The parameters were transitioned from the SMS material model in Set A to the EMS material model in Set C. The results of Set C had three differences compared to Set A and these differences were consistent across all loading rates:

1) The slope in the initial loading regime was steeper,
2) failure occurred at higher peak stress, and
3) failure occurred at lower values of normalized displacement.

To reconcile all three of these differences we had to change the TSLs and also two of the parameters from the EMS material model. We note that for the Tensylon composites (Alexander et al. 2023a), we were able to match the experimental response with the EMS material model by only making a few adjustments to the shape of the TSLs without having to make any changes to the parameters of the EMS material model. We avoided having to make changes to the EMS parameters for the Tensylon composites because transitioning the parameters from the SMS material model to the EMS material model (from Set A to Set C) caused only an increase in peak stress without the other two changes that were observed here for the fiber-based composites.

5.2 Shape of the TSLs

We previously simulated OALS experiments on film-based composites using one of the prepackaged options for tiebreaking in LS-DYNA. That option was based on the TSL being triangular in shape. We tried to use this same option for the present fiber-based composites in preliminary simulations. However, in the simulations with this option, the downward slope of the load-displacement curve after peak load was too steep relative to the experiments. Appendix C provides some examples. Therefore, we next tried the LS-DYNA prepackaged option for a traction-separation that was trapezoidal in shape. We thought we would be able to match the gradual post-peak response observed in the experiments by extending the plateau at the top of the trapezoid. However, as shown in the examples in Appendix C, these trapezoidal TSLs still caused the load-displacement response to drop too precipitously after peak. We concluded that we needed to be able to implement our own custom-shaped TSL in order to match the gradual load decay shown in the experiments.

Appendix A provides examples of the many iterations that were necessary to fine-tune the shape of the TSL to match the response of the experiments. Sometimes changes to the shape of the TSL did not affect the load-displacement response over the displacement regimes in the OALS simulations. Appendix A provides several examples of such cases.

5.3 Rate Dependence of Simulation Parameters

When simulated in a multiaxial loading condition, as can be expected in simulations where the UHMWPE material interacts with materials of other systems, each element in the UHMWPE will be experiencing a different strain rate. Therefore, ideally our computational framework would be based entirely on rate-dependent models. Currently, only the plasticity component (Eq. 1) explicitly includes rate-dependence. The elasticity component of the SMS model as well as the TSLs required values to be identified at each rate, as listed in Table 3. Figure 10 plots the rate dependence of the values from Table 3 and compares them to the values we previously found for Tensylon composites.

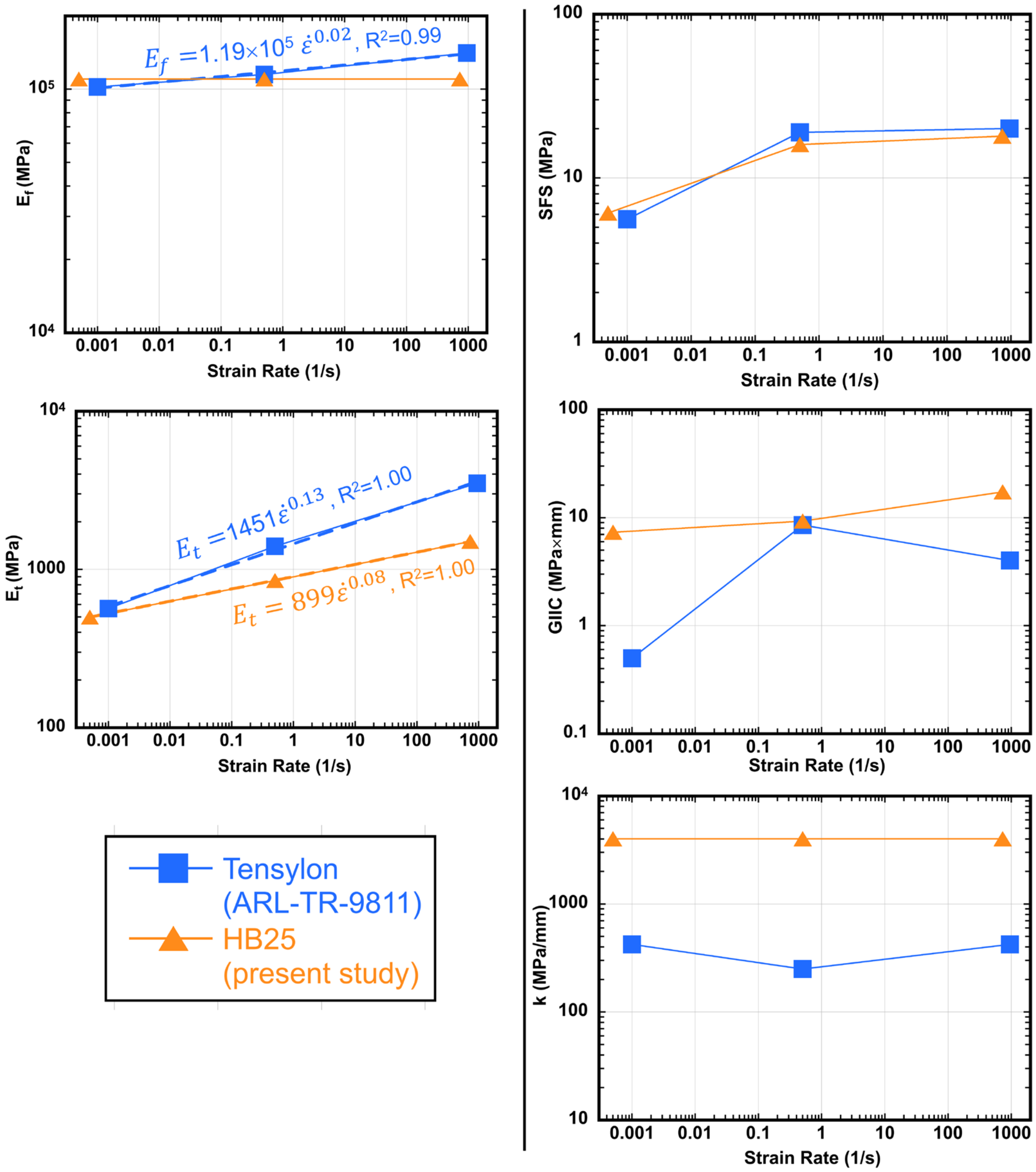

Fig. 10 Log–log plots of the FE simulation parameters identified using the SMS model (Set A) against strain rate for HB25 fiber-based composites (present study) and Tensylon film-based composites (Alexander et al. 2023a). Plots in the left column are elastic constants from the SMS material model and include the fitted power law equation where applicable. Plots in the right column are from the TSLs.

In the SMS material model, the transverse modulus, E_t, had a dependence on rate on the order of $E_t = 1.0\dot{\varepsilon}^{0.1}$ GPa, which was approximately consistent with the film-based composites (Fig. 10). The failure strength for Mode 2 delamination (SFS) increased from LR to IR but then did not further increase with rate from IR to HR. The same phenomenon has been previously observed in experiments on single SK76 UHMWPE fibers (Sanborn et al. 2015) and SK76 yarns (Russell et al. 2013). The GIIC value had an unclear dependence on rate, especially when considering the limitations on this parameter as discussed in Section 5.5. SFS increases from LR to IR and then plateaus. The remaining parameters were, and can be assumed as, approximately rate-independent.

5.4 Contributions from Each Slip System

The contribution of each slip system in the SMS model, α, to the overall response was quantified by rerunning the Set B simulation at IR. While rerunning, the cumulative shear strain increment from each slip system, $\Delta\gamma^{\alpha}$, was saved during the simulation. The shear strain increment was defined as the shear strain rate, $\dot{\gamma}$, given in Eq. 1 multiplied by Δt, the size of the current time increment:

$$\Delta\gamma^{\alpha} = \dot{\gamma}^{\alpha}\Delta t \tag{7}$$

Figure 11 presents the cumulative $\Delta\gamma^{\alpha}$ from representative elements within 0° and 90° layers. In each layer, there is only one or two dominant slip systems that account for the majority of the shearing. Figure 4 describes the slip systems for a 0° layer. For the 0° layer, slip system $\alpha = 2$ was dominant, while slip systems 1, 3, and 4 were not active. For the 90° layer, slip systems $\alpha = 3$ and $\alpha = 4$ were dominant, with equal contributions, while slip systems 1 and 2 were not active. The shear strain on systems $\alpha = 3$ and $\alpha = 4$ were equal because they are orthogonal slip systems that experience the same shear stress and consequently produce the same shear strain.

The two additional slip systems that differentiated the fiber-based materials from the film-based materials simulated in Alexander et al. (2023a) were $\alpha = 5$ and $\alpha = 6$. These two systems were active in both the 0° and 90° layers. In addition, the contributions from $\alpha = 5$ and $\alpha = 6$ were equal in magnitude, which may be related to the in-plane deviatoric strain accompanying the volume compression. With reference to the schematic of the slip systems (Fig. 4), through-thickness compression of the UD layer in the global 3-direction would be accommodated by these two systems ($\alpha = 5$ and $\alpha = 6$) acting together. In the 0° layer, the contributions from these two systems had opposite signs (Fig. 11, left) and therefore offset each other. In the 90° layer, the contributions had the same sign (Fig. 11, right) and were therefore additive.

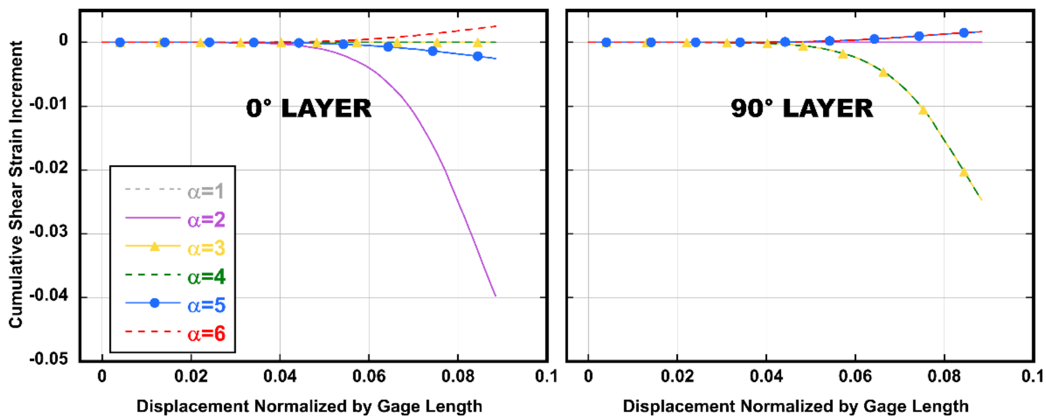

Fig. 11 The cumulative shear strain increment (Eq. 7) from each slip system during the Set B simulation at IR. Data collected from representative elements near center of specimen.

5.5 Limitations

The methods used here to identify the FE parameters for simulating the fiber-based composites were analogous to our previous work on simulating film-based composites reported in Alexander et al. (2023a). The limitations of these methods were previously documented in detail for the film-based composites and were also applicable to the present simulations. Here we only reiterate that a central limitation was that the method for determining the parameter values was not unique. An example was the choice of which parameters to assume constant and which values to optimize. Different choices may have yielded similar results. In particular, both E_t and G_{ft} may contribute to the stiffness. We chose to adjust the slope of the initial elastic regime by changing E_t while keeping G_{ft} fixed at the value that was determined experimentally and subsequently successfully used in simulations by a research group at Cambridge University (Atwood et al. 2014; Liu et al. 2014, 2019; Varun Raj et al. 2022). We found that E_t had a more noticeable and direct effect on the stiffness, whereas G_{ft} did not appear to directly affect the stiffness (see Appendix B).

There were additional limitations that arose for the fiber-based composites due to the method of modeling inter-laminar delamination. First, as discussed previously and shown in Appendix A, sometimes different shapes of the TSL resulted in the same load-displacement curves. Therefore, the total area of the curve, GIIC, is not a unique parameter and any comparison between simulations of GIIC values should be critically evaluated. In addition, the contact algorithms in LS-DYNA that were employed via the particular combination of keywords used in these simulations (Section 3.5) did not work after the elements had separated by a distance of more than one element length from each other. After this point, the results were nonphysical and seemed to indicate numerical breakdown. Additional research could be done to identify other options within LS-DYNA for contact to try to extend the capability of modeling delamination beyond one element length, but this was outside the scope of the present work.

6. Conclusions and Transitional Outcomes

6.1 Summary of Findings

The subscale computational framework that was previously developed for simulating failure by shear delamination failure mechanism in film-based UHMWPE composites loaded in off-axis shear was successfully adapted for similarly loaded fiber-based composites.

The fiber-based composites were relatively more difficult to simulate than the film-based composites. Whereas, before we were able to match the experimental response with the triangular TSL in LS-DYNA, here we had to develop the capability for using our own custom-defined shape. Before, with film-based laminates, we were able to take the values that defined the plastic slip rate almost directly from the experimental results, but for the fiber-based composites we had to iterate on those parameters to match experimental plastic response. Moreover, with the film-based composites, we were able to transition parameters directly from the SMS to the EMS material models; subsequent optimizing only involved changes to the shape of the triangular TSL but not to the EMS material model. On the contrary, with the present fiber-based composites, we not only had to change the shape of the TSLs, but we also had to adjust the values of some of the parameters within the EMS deformation model.

6.2 Transitional Outcomes

Other researchers can use the capability that was developed here for implementing a custom-shaped traction–separation relationship in LS-DYNA. The prebuilt options in LS-DYNA for triangular and trapezoidal TSL shapes caused the loading response to drop too precipitously after reaching the peak. Therefore, other researchers with materials that also show a gradual decline in load after reaching the peak, rather than a steep drop off, may also benefit from using this developed somewhat generalized capability to create their own TSL shapes. Appendix D provides instructions on how to set up the LS-DYNA input file to use the user-defined tiebreak model that we developed here.

Researchers can use the reported optimized parameters for the EMS model (Tables 4 and 5) in simulations involving large multiple interacting material systems in which modeling each UD layer of UHMWPE would be impractical. These EMS parameters had been obtained using our subscale (SMS) material model. With the parameters in Table 5, the EMS model was shown to satisfactorily represent the experimental load-displacement response and the finally observed sheared rhombic shape of the deformed specimen. Appendixes E and F provide simplified instructions on how to set up the LS-DYNA input file to run the SMS and EMS models, respectively.

At present, we recommend that while simulating scenarios with dynamic loading, such as ballistic events, researchers use the high-rate parameters listed in Tables 4 and 5. The instructions provided in Appendixes D through F are based on these high-rate parameters. In future versions, the present computational framework could be extended by incorporating the observed power-law rate-dependent models for elasticity; and for delamination, use the average values for cohesive failure constants (GIIC, k, and SFS). This would obviate the need for having a different set of parameters for each rate as different elements deform under different strain rates.

7. References

Alexander SL, Becker R, Weerasooriya T. An experimental-computational framework for UHMWPE films based on deformation and failure mechanisms: general approach and application to off-axis shear loading. DEVCOM Army Research Laboratory (US); 2023a Oct. Report No.: ARL-TR-9811. https://apps.dtic.mil/sti/trecms/pdf/AD1213059.pdf

Alexander SL, Becker R, Weerasooriya T. User guide to a wrapper that allows a custom user-defined material model (UMAT) originally developed for Abaqus/EPIC to be used in LS-DYNA simulations. DEVCOM Army Research Laboratory (US); 2023b Oct. Report No.: ARL-TN-1177. https://apps.dtic.mil/sti/trecms/pdf/AD1214015.pdf

Alexander SL, Weerasooriya T. Mechanical characterization of advanced ultra-high molecular weight polyethylene (UHMWPE) composites by ultrasonic method. DEVCOM Army Research Laboratory (US); 2021 Aug. Report No.: ARL-TR-9254. https://apps.dtic.mil/sti/pdfs/AD1146645.pdf

Atwood JP, Khaderi SN, Karthikeyan K, Fleck NA, O'Masta MR, Wadley HNG, Deshpande VS. The out-of-plane compressive response of Dyneema composites. J Mech and Phys of Solids. 2014;70:200–226.

Becker R. Investigation of slip kinematics in an ultra-high molecular weight polyethylene (UHMWPE) laminar composite model. DEVCOM Army Research Laboratory (US); 2019 Dec. Report No.: ARL-TN-0985. https://apps.dtic.mil/sti/pdfs/AD1087651.pdf

Cline J, Love B. The effect of in-plane shear properties on the ballistic performance of polyethylene composites. Int J Impact Eng. 2020;143:103592.

Freitas CJ, Bigger RP, Scott N, LaSala V, MacKiewicz J. Composite materials dynamic back face deflection characteristics during ballistic impact. J Compos Mater. 2014;48(12):1475–1486.

Gunnarsson CA, Alexander SL, Weerasooriya T. Rate dependent shear response during off-axis loading of fiber and film-based UHMWPE composites. DEVCOM Army Research Laboratory (US); 2023 Oct. Report No.: ARL-TR-9813. https://apps.dtic.mil/sti/trecms/pdf/AD1213062.pdf

Hoppel C, Stepp D, Becker R, Bakas M, Vargas-Gonzales L, Tonge A, Tschopp M. Controlling the load distribution in high-strength materials Army science planning and strategy meeting (ASPSM). DEVCOM Army Research

Laboratory (US); 2021 Feb. Report No.: ARL-SR-0438. https://apps.dtic.mil/sti/pdfs/AD1123267.pdf

Liu G, Thouless MD, Deshpande VS, Fleck NA. Collapse of a composite beam made from ultra high molecular-weight polyethylene fibres. J Mech and Phys of Solids. 2014;63:320–335.

Liu BG, Wadley HN, Deshpande VS. Failure mechanism maps for ultra-high molecular weight polyethylene fibre composite beams impacted by blunt projectiles. Int J Solids Struct. 2019;178:180–198.

LS-DYNA. LS-DYNA keyword user's manual volume I, II. Ver. R14.0. ANSYS; 2023 Feb 24.

Reddy PR, Reddy TS, Srikanth I, Kushwaha J, Madhu V. Development of cost effective personnel armour through structural hybridization. Defence Tech. 2020;16(6):1089–1097.

Russell BP, Karthikeyan K, Deshpande VS, Fleck NA. The high strain rate response of ultra high molecular weight polyethylene: from fibre to laminate. 2013;60:1–9.

Sanborn B, DiLeonardi AM, Weerasooriya T. Tensile properties of Dyneema SK76 single fibers at multiple loading rates using a direct gripping method. J Dynamic Behavior Mater. 2015;1(1):4–14. doi:10.1007/s40870-014-0001-3.

Varun Raj R, Liu BG, Peerlings RHJ, Deshpande VS. Influence of microstructure on the failure of ultra-high molecular weight polyethylene composite beams impacted by blunt projectiles. Mechanics of Materials. 2022;164:104106.

Appendix A. Repository of Examples Captured from Optimization Process Demonstrating the Effect of the Customized Shape of the Traction-Separation Law (TSL) on the Load-Displacement Response

This Appendix is a repository of several examples captured during the iterative process that was used to identify the shape of the TSL. The examples are presented without further organization and are from preliminary simulations that also differed in other details from the Sets A–D simulations. The examples are meant only to provide a qualitative understanding of the effect of the shape of the TSLs on the mechanical response for the reader seeking further detail.

Each figure in this Appendix consists of a pair of two subfigures. The larger subfigure on the left compares the load-displacement response of the experiment (black dotted line) and the simulations (solid lines of different colors). The inset subfigure on the right shows the shape of the TSLs for each of the simulations, with the TSLs color-coded against the simulations in the load-displacement figure.

Section A.1 provides examples showing changes in the TSL that caused noticeable effects on the load-displacement response. Section A.2 shows instances when changes in the TSL did not substantially affect the load-displacement response.

A.1 Examples Showing How Load-Displacement Response Changes with TSL

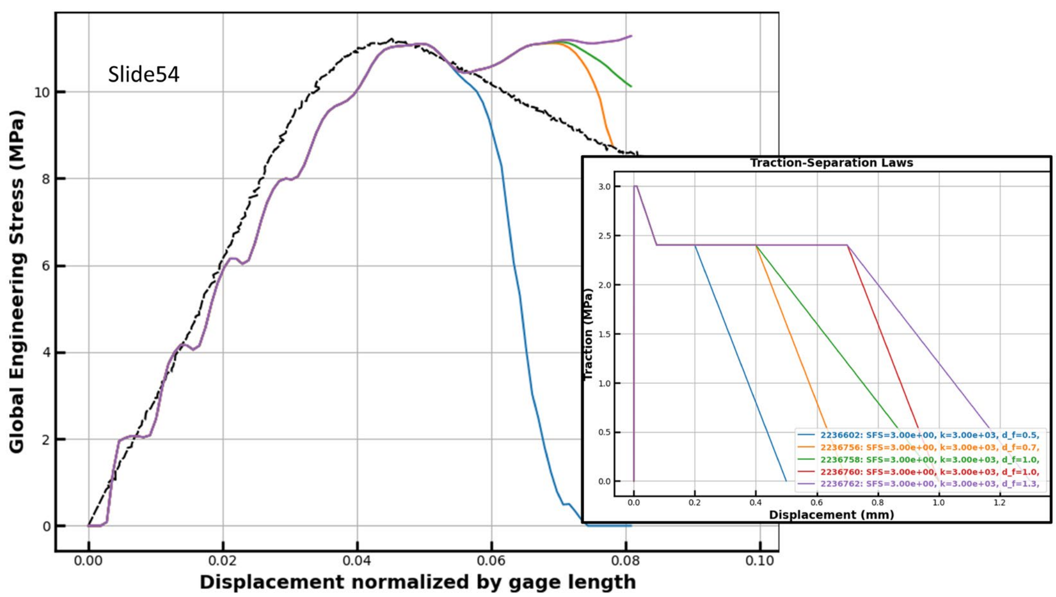

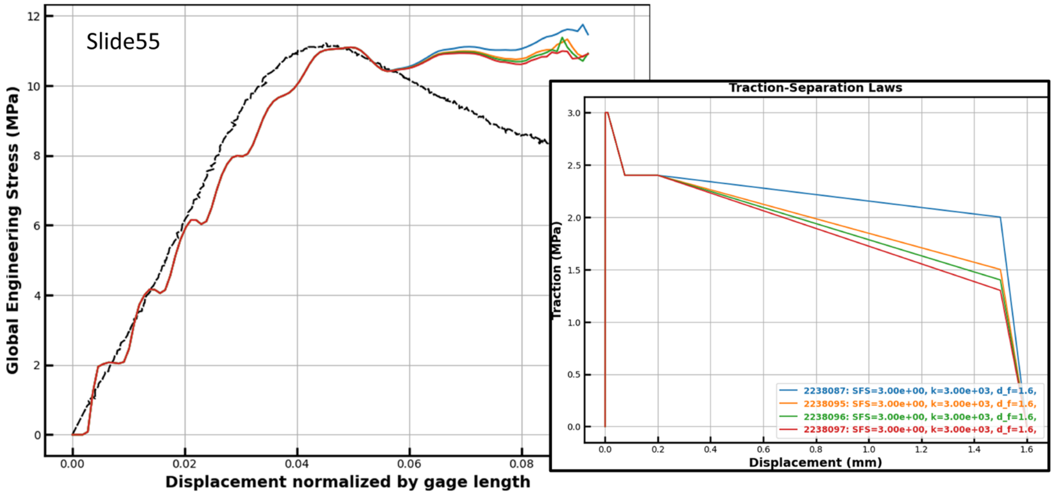
Slide55
Global Engineering Stress (MPa)
Displacement normalized by gage length
Traction-Separation Laws
Traction (MPa)
Displacement (mm)
2238087: SFS=3.00e+00, k=3.00e+03, d_f=1.6,
2238095: SFS=3.00e+00, k=3.00e+03, d_f=1.6,
2238096: SFS=3.00e+00, k=3.00e+03, d_f=1.6,
2238097: SFS=3.00e+00, k=3.00e+03, d_f=1.6,

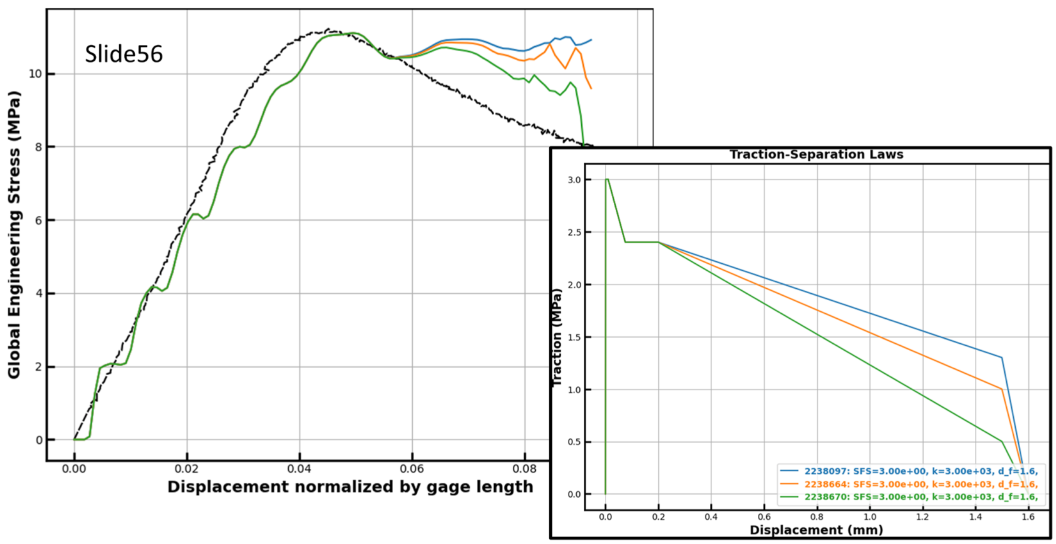
Slide56
Global Engineering Stress (MPa)
Displacement normalized by gage length
Traction-Separation Laws
Traction (MPa)
Displacement (mm)
2238097: SFS=3.00e+00, k=3.00e+03, d_f=1.6,
2238664: SFS=3.00e+00, k=3.00e+03, d_f=1.6,
2238670: SFS=3.00e+00, k=3.00e+03, d_f=1.6,

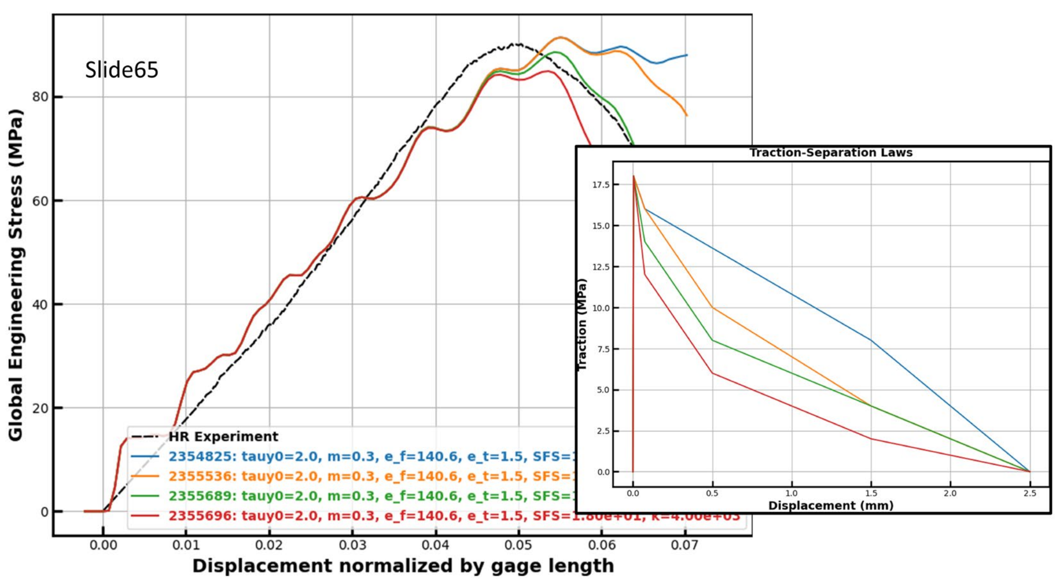
Slide65
Global Engineering Stress (MPa)
Displacement normalized by gage length
HR Experiment
2354825: tauy0=2.0, m=0.3, e_f=140.6, e_t=1.5, SFS=
2355536: tauy0=2.0, m=0.3, e_f=140.6, e_t=1.5, SFS=
2355689: tauy0=2.0, m=0.3, e_f=140.6, e_t=1.5, SFS=
2355696: tauy0=2.0, m=0.3, e_f=140.6, e_t=1.5, SFS=1.80e+01, k=4.00e+03
Traction-Separation Laws
Traction (MPa)
Displacement (mm)

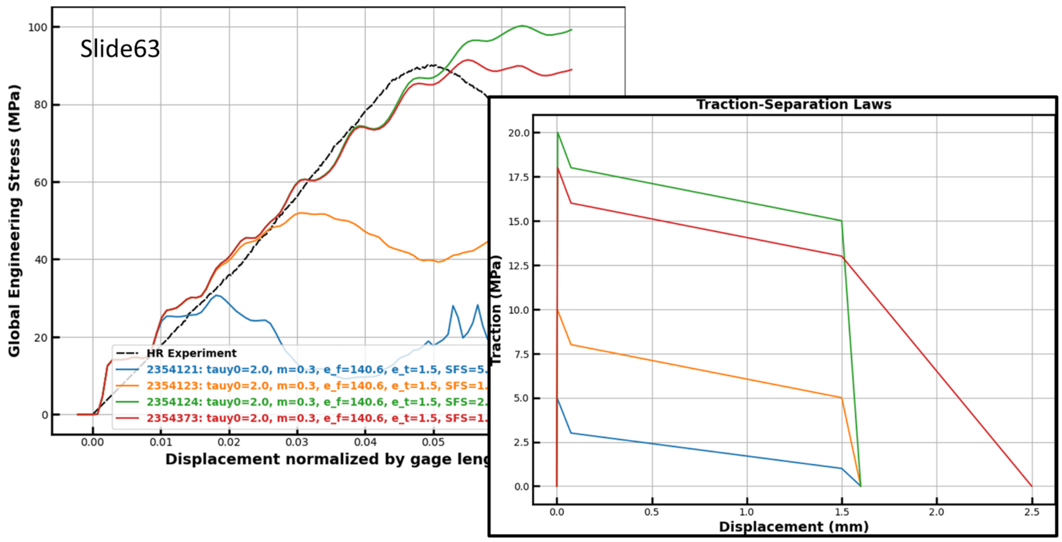
Slide63
Global Engineering Stress (MPa)
Displacement normalized by gage leng
HR Experiment
2354121: tauy0=2.0, m=0.3, e_f=140.6, e_t=1.5, SFS=5.
2354123: tauy0=2.0, m=0.3, e_f=140.6, e_t=1.5, SFS=1.
2354124: tauy0=2.0, m=0.3, e_f=140.6, e_t=1.5, SFS=2.
2354373: tauy0=2.0, m=0.3, e_f=140.6, e_t=1.5, SFS=1.
Traction-Separation Laws
Traction (MPa)
Displacement (mm)

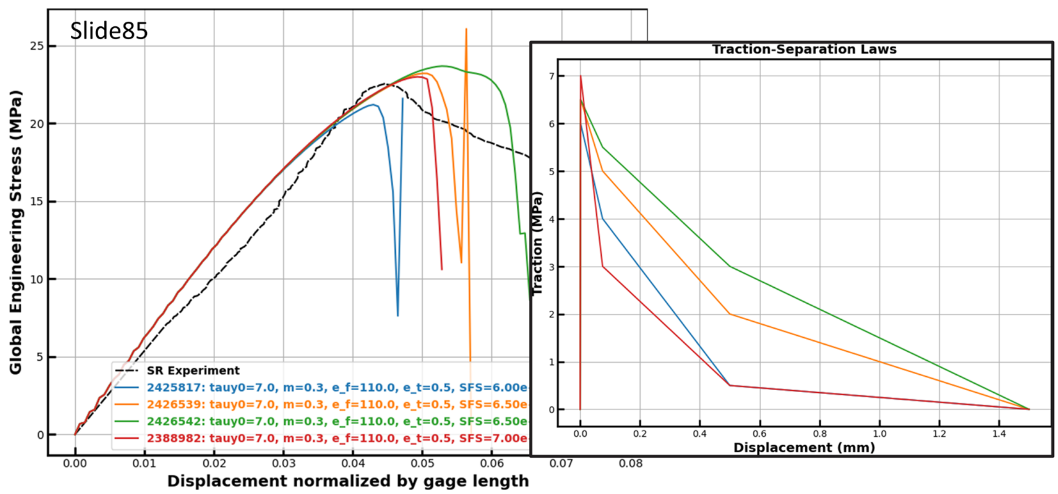
Slide85
Global Engineering Stress (MPa)
Displacement normalized by gage length
SR Experiment
2425817: tauy0=7.0, m=0.3, e_f=110.0, e_t=0.5, SFS=6.00e
2426539: tauy0=7.0, m=0.3, e_f=110.0, e_t=0.5, SFS=6.50e
2426542: tauy0=7.0, m=0.3, e_f=110.0, e_t=0.5, SFS=6.50e
2388982: tauy0=7.0, m=0.3, e_f=110.0, e_t=0.5, SFS=7.00e
Traction-Separation Laws
Traction (MPa)
Displacement (mm)

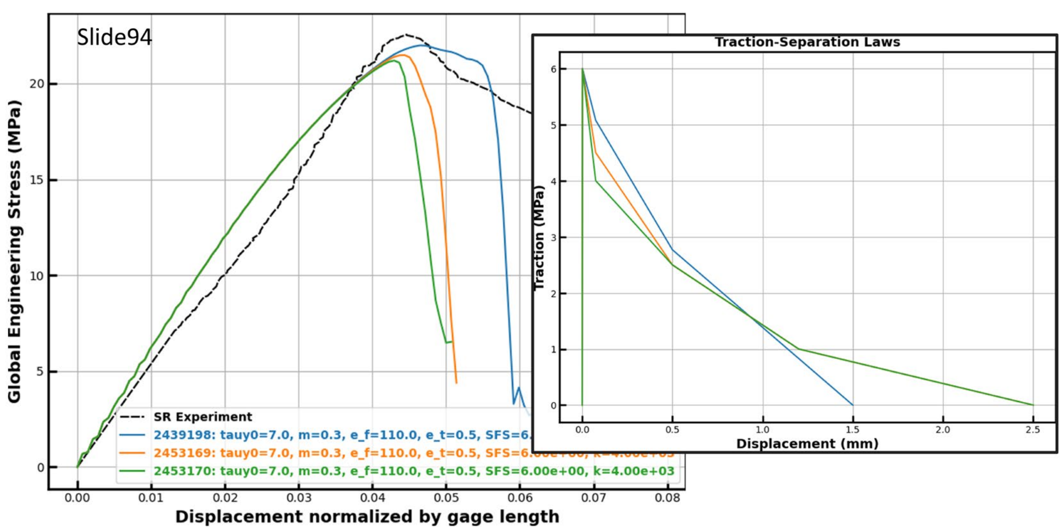
Slide94
Global Engineering Stress (MPa)
Displacement normalized by gage length
SR Experiment
2439198: tauy0=7.0, m=0.3, e_f=110.0, e_t=0.5, SFS=6.
2453169: tauy0=7.0, m=0.3, e_f=110.0, e_t=0.5, SFS=6
2453170: tauy0=7.0, m=0.3, e_f=110.0, e_t=0.5, SFS=6.00e+00, k=4.00e+03
Traction-Separation Laws
Traction (MPa)
Displacement (mm)

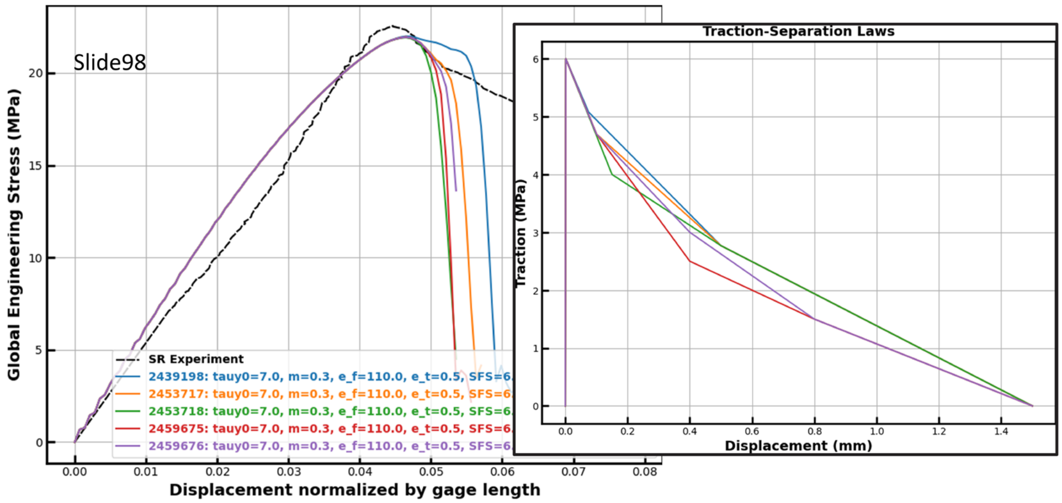

Slide98
Global Engineering Stress (MPa)
Displacement normalized by gage length
SR Experiment
2439198: tauy0=7.0, m=0.3, e_f=110.0, e_t=0.5, SFS=6.
2453717: tauy0=7.0, m=0.3, e_f=110.0, e_t=0.5, SFS=6.
2453718: tauy0=7.0, m=0.3, e_f=110.0, e_t=0.5, SFS=6.
2459675: tauy0=7.0, m=0.3, e_f=110.0, e_t=0.5, SFS=6.
2459676: tauy0=7.0, m=0.3, e_f=110.0, e_t=0.5, SFS=6.
Traction-Separation Laws
Traction (MPa)
Displacement (mm)

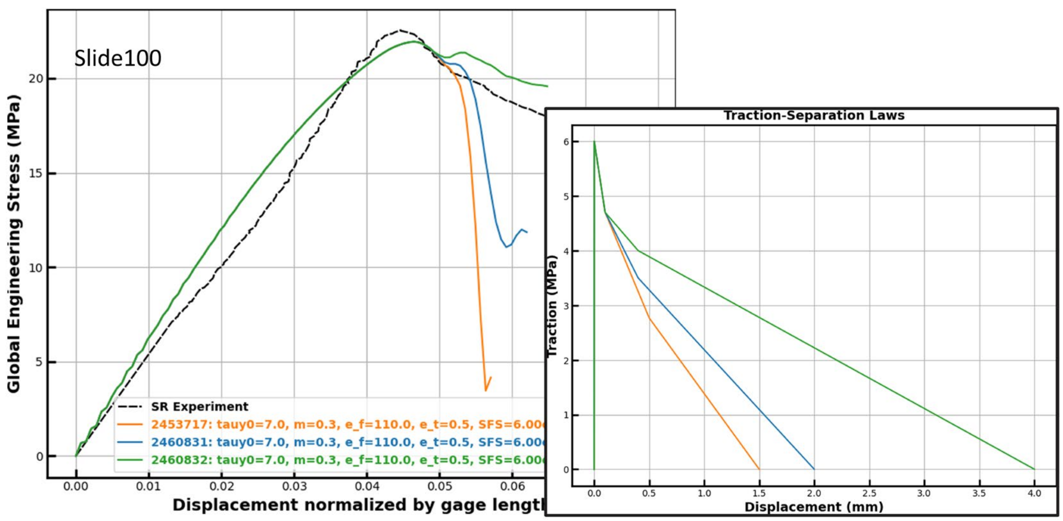

Slide100
Global Engineering Stress (MPa)
Displacement normalized by gage length
SR Experiment
2453717: tauy0=7.0, m=0.3, e_f=110.0, e_t=0.5, SFS=6.00
2460831: tauy0=7.0, m=0.3, e_f=110.0, e_t=0.5, SFS=6.00
2460832: tauy0=7.0, m=0.3, e_f=110.0, e_t=0.5, SFS=6.00
Traction-Separation Laws
Traction (MPa)
Displacement (mm)

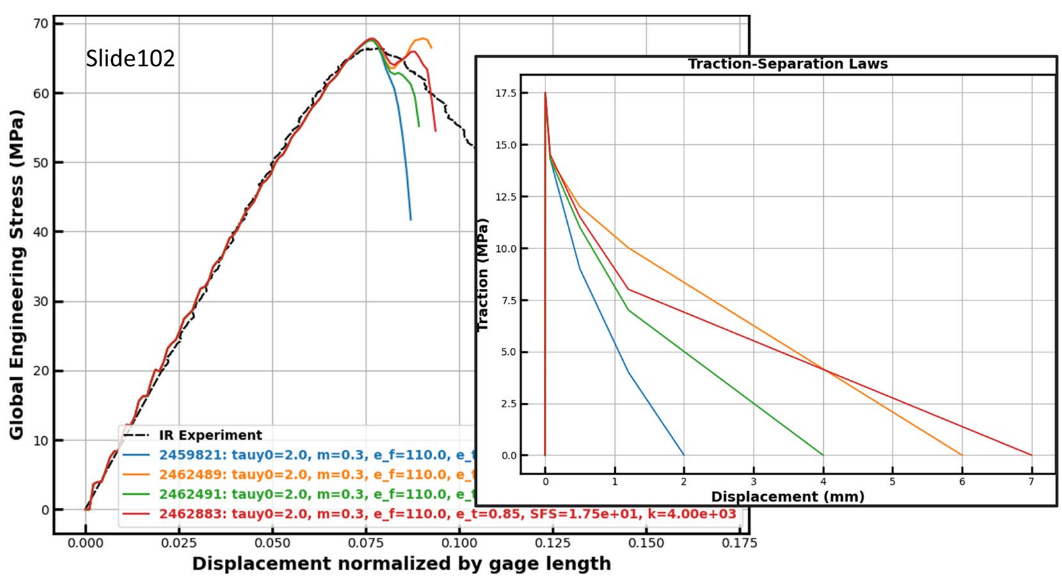

Slide102
Global Engineering Stress (MPa)
Displacement normalized by gage length
IR Experiment
2459821: tauy0=2.0, m=0.3, e_f=110.0, e_
2462489: tauy0=2.0, m=0.3, e_f=110.0, e_
2462491: tauy0=2.0, m=0.3, e_f=110.0, e_
2462883: tauy0=2.0, m=0.3, e_f=110.0, e_t=0.85, SFS=1.75e+01, k=4.00e+03
Traction-Separation Laws
Traction (MPa)
Displacement (mm)

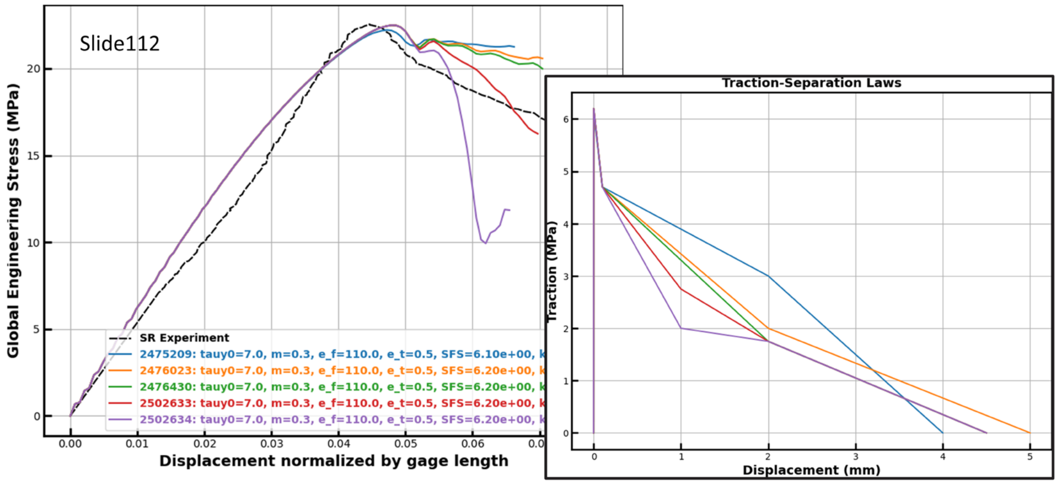
Slide112
Global Engineering Stress (MPa)
Displacement normalized by gage length
SR Experiment
2475209: tauy0=7.0, m=0.3, e_f=110.0, e_t=0.5, SFS=6.10e+00, k
2476023: tauy0=7.0, m=0.3, e_f=110.0, e_t=0.5, SFS=6.20e+00, k
2476430: tauy0=7.0, m=0.3, e_f=110.0, e_t=0.5, SFS=6.20e+00, k
2502633: tauy0=7.0, m=0.3, e_f=110.0, e_t=0.5, SFS=6.20e+00, k
2502634: tauy0=7.0, m=0.3, e_f=110.0, e_t=0.5, SFS=6.20e+00, k
Traction-Separation Laws
Traction (MPa)
Displacement (mm)

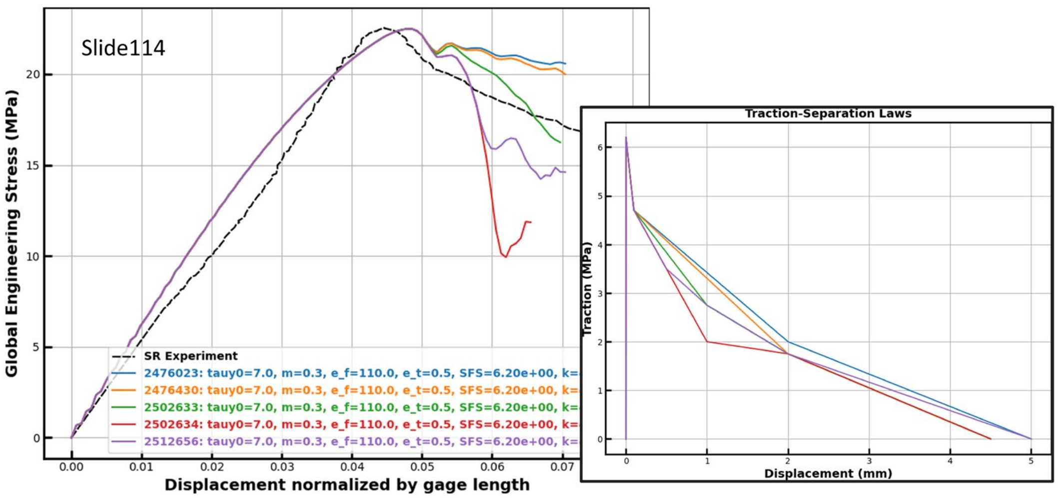
Slide114
Global Engineering Stress (MPa)
Displacement normalized by gage length
SR Experiment
2476023: tauy0=7.0, m=0.3, e_f=110.0, e_t=0.5, SFS=6.20e+00, k=
2476430: tauy0=7.0, m=0.3, e_f=110.0, e_t=0.5, SFS=6.20e+00, k=
2502633: tauy0=7.0, m=0.3, e_f=110.0, e_t=0.5, SFS=6.20e+00, k=
2502634: tauy0=7.0, m=0.3, e_f=110.0, e_t=0.5, SFS=6.20e+00, k=
2512656: tauy0=7.0, m=0.3, e_f=110.0, e_t=0.5, SFS=6.20e+00, k=
Traction-Separation Laws
Traction (MPa)
Displacement (mm)

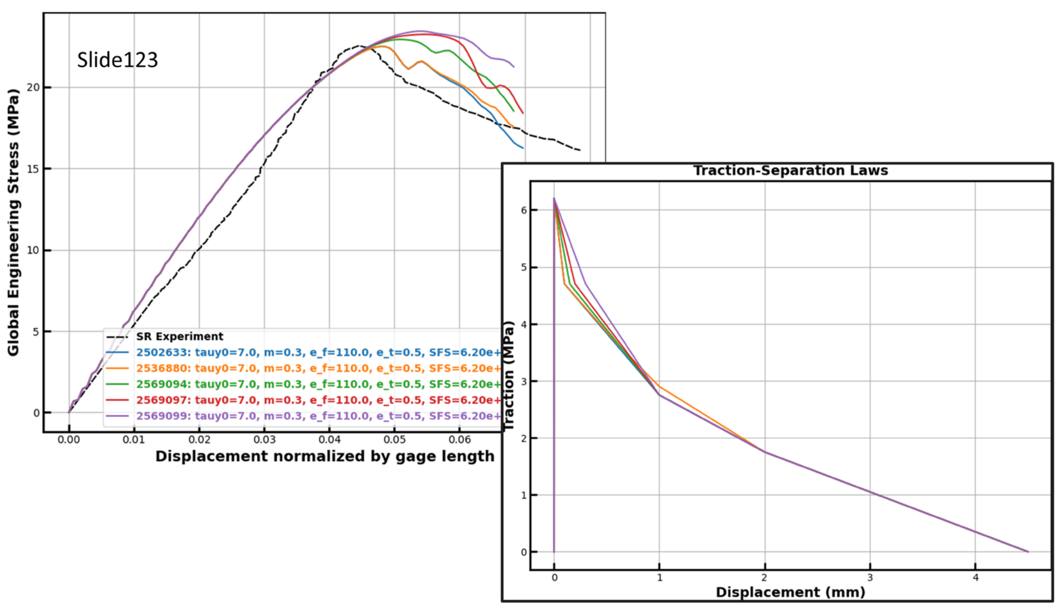
Slide123
Global Engineering Stress (MPa)
Displacement normalized by gage length
SR Experiment
2502633: tauy0=7.0, m=0.3, e_f=110.0, e_t=0.5, SFS=6.20e+
2536880: tauy0=7.0, m=0.3, e_f=110.0, e_t=0.5, SFS=6.20e+
2569094: tauy0=7.0, m=0.3, e_f=110.0, e_t=0.5, SFS=6.20e+
2569097: tauy0=7.0, m=0.3, e_f=110.0, e_t=0.5, SFS=6.20e+
2569099: tauy0=7.0, m=0.3, e_f=110.0, e_t=0.5, SFS=6.20e+
Traction-Separation Laws
Traction (MPa)
Displacement (mm)

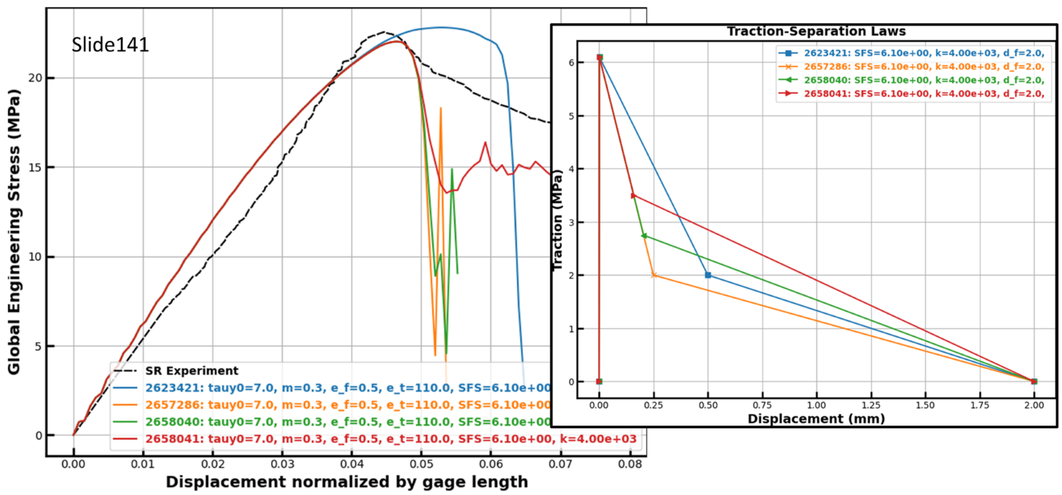

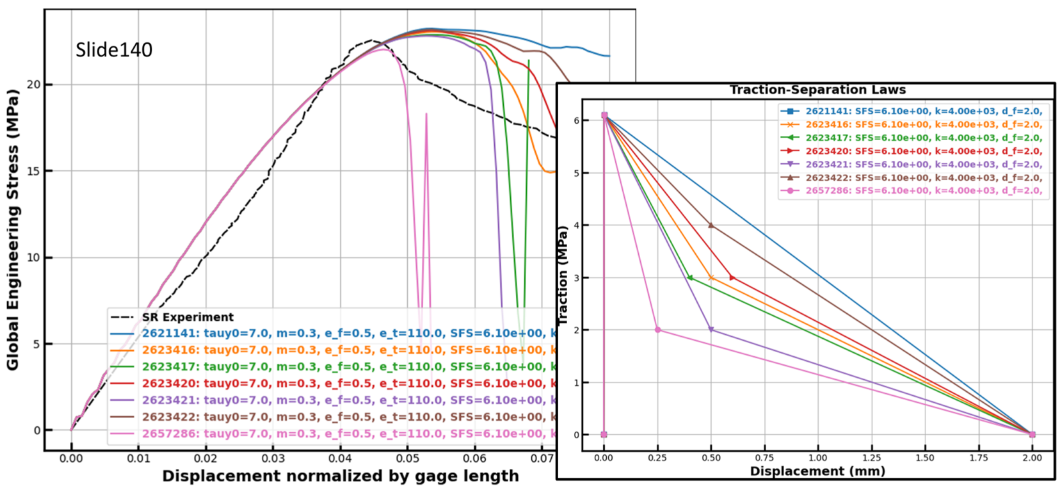

A.2 Examples of Changes in TSL Shape that did not Substantially Affect the Load-Displacement Response

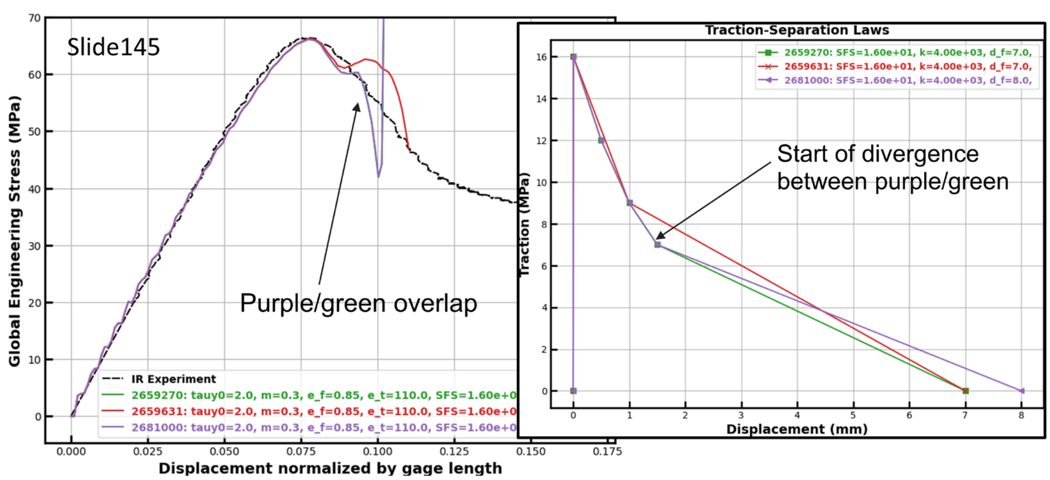

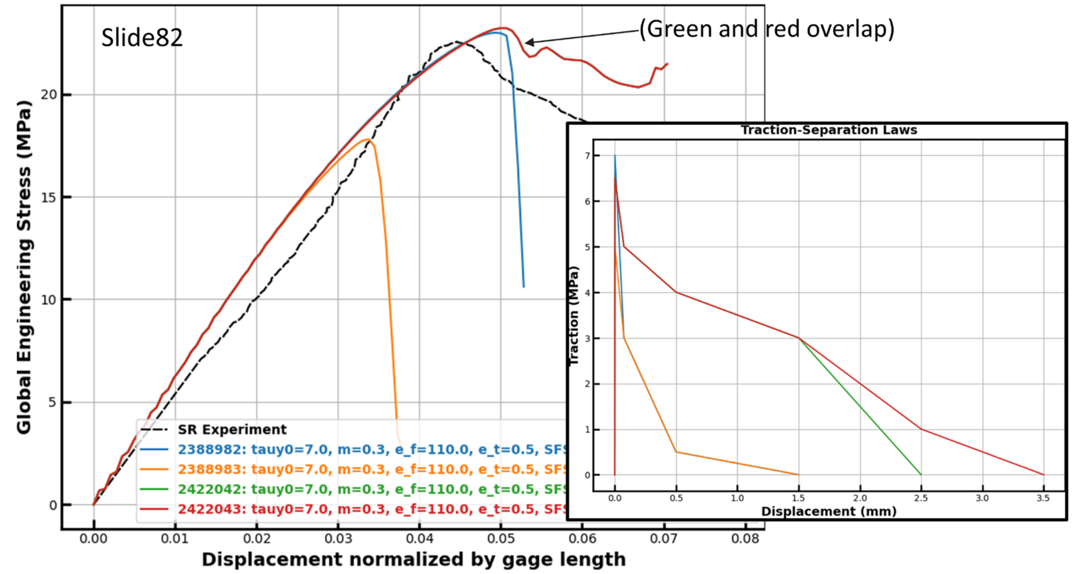

Slide82
(Green and red overlap)
Global Engineering Stress (MPa)
Displacement normalized by gage length
SR Experiment
2388982: tauy0=7.0, m=0.3, e_f=110.0, e_t=0.5, SF
2388983: tauy0=7.0, m=0.3, e_f=110.0, e_t=0.5, SF
2422042: tauy0=7.0, m=0.3, e_f=110.0, e_t=0.5, SF
2422043: tauy0=7.0, m=0.3, e_f=110.0, e_t=0.5, SF
Traction-Separation Laws
Traction (MPa)
Displacement (mm)

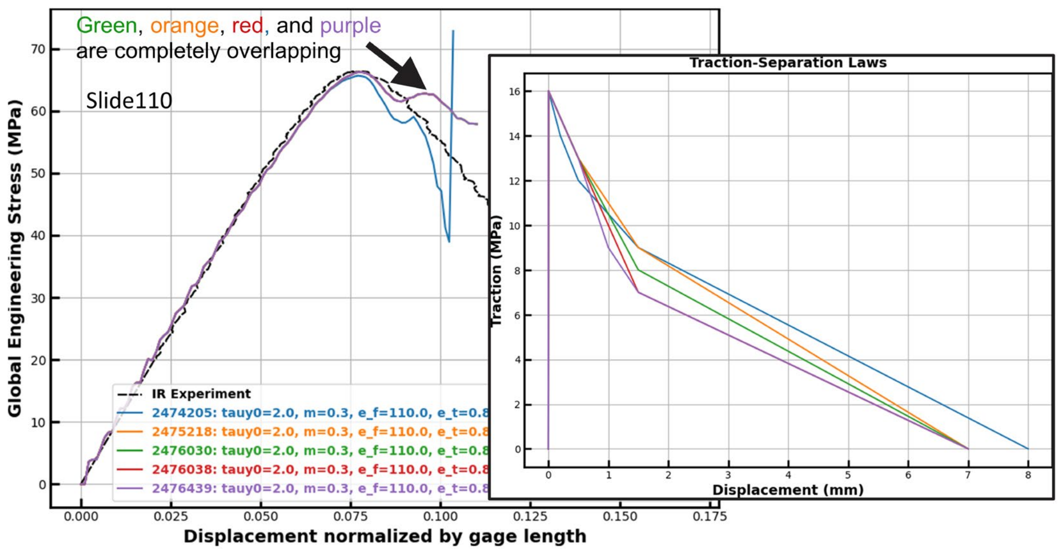

Green, orange, red, and purple
are completely overlapping
Slide110
Global Engineering Stress (MPa)
Displacement normalized by gage length
IR Experiment
2474205: tauy0=2.0, m=0.3, e_f=110.0, e_t=0.8
2475218: tauy0=2.0, m=0.3, e_f=110.0, e_t=0.8
2476030: tauy0=2.0, m=0.3, e_f=110.0, e_t=0.8
2476038: tauy0=2.0, m=0.3, e_f=110.0, e_t=0.8
2476439: tauy0=2.0, m=0.3, e_f=110.0, e_t=0.8
Traction-Separation Laws
Traction (MPa)
Displacement (mm)

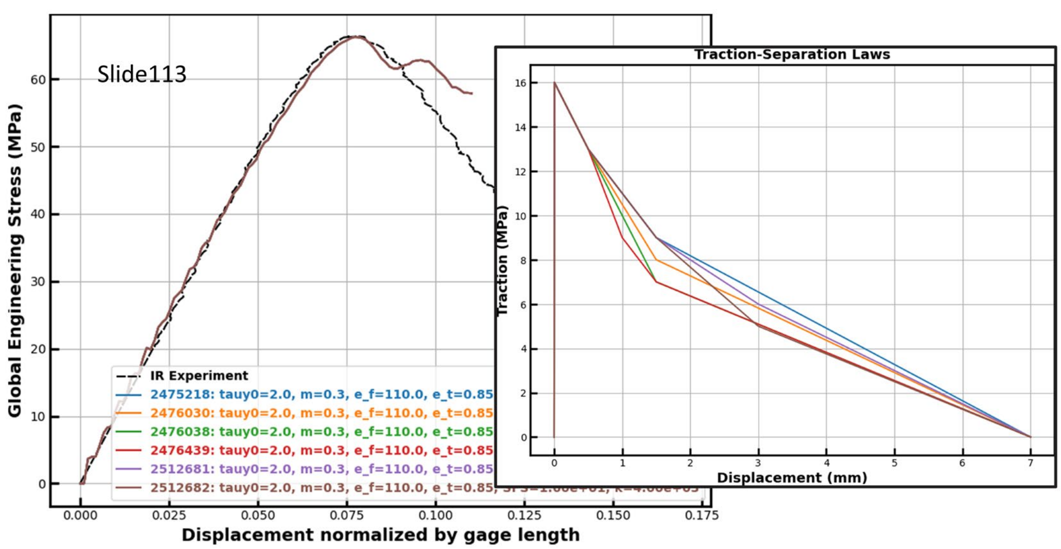

Slide113
Global Engineering Stress (MPa)
Displacement normalized by gage length
IR Experiment
2475218: tauy0=2.0, m=0.3, e_f=110.0, e_t=0.85
2476030: tauy0=2.0, m=0.3, e_f=110.0, e_t=0.85
2476038: tauy0=2.0, m=0.3, e_f=110.0, e_t=0.85
2476439: tauy0=2.0, m=0.3, e_f=110.0, e_t=0.85
2512681: tauy0=2.0, m=0.3, e_f=110.0, e_t=0.85
2512682: tauy0=2.0, m=0.3, e_f=110.0, e_t=0.85
Traction-Separation Laws
Traction (MPa)
Displacement (mm)

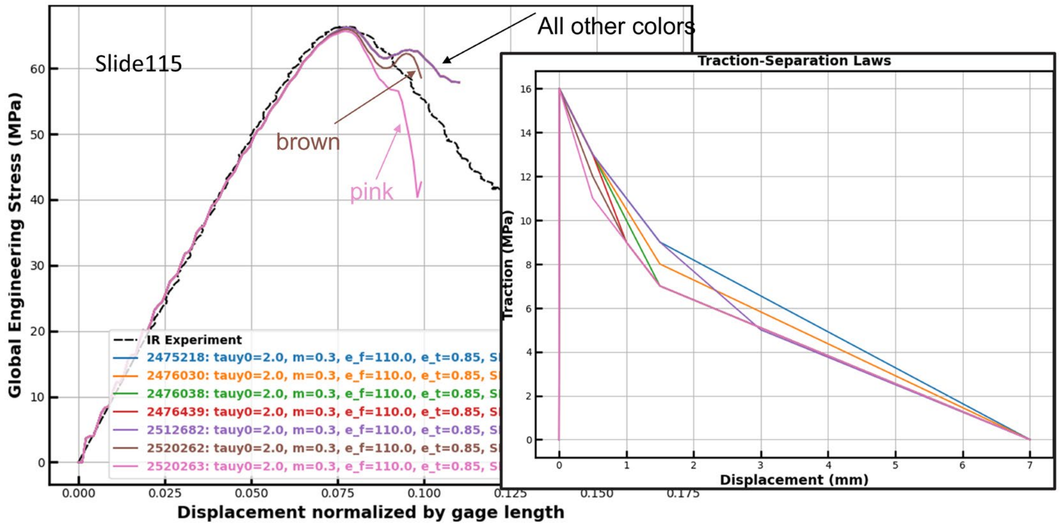
Slide115
All other colors
brown
pink
Global Engineering Stress (MPa)
Displacement normalized by gage length
IR Experiment
2475218: tauy0=2.0, m=0.3, e_f=110.0, e_t=0.85, S
2476030: tauy0=2.0, m=0.3, e_f=110.0, e_t=0.85, S
2476038: tauy0=2.0, m=0.3, e_f=110.0, e_t=0.85, S
2476439: tauy0=2.0, m=0.3, e_f=110.0, e_t=0.85, S
2512682: tauy0=2.0, m=0.3, e_f=110.0, e_t=0.85, S
2520262: tauy0=2.0, m=0.3, e_f=110.0, e_t=0.85, S
2520263: tauy0=2.0, m=0.3, e_f=110.0, e_t=0.85, S
Traction-Separation Laws
Traction (MPa)
Displacement (mm)

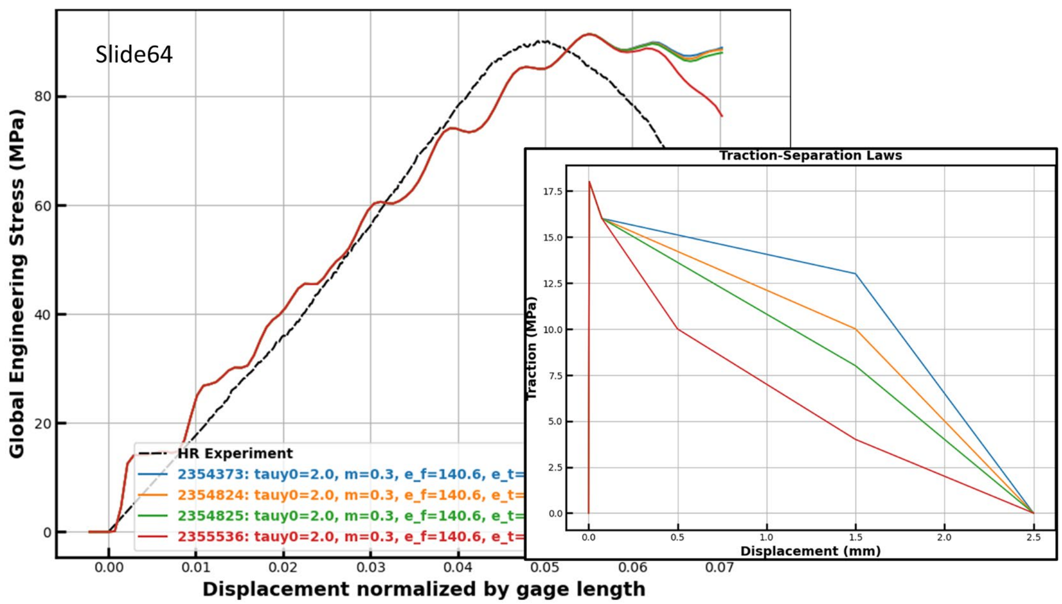
Slide64
Global Engineering Stress (MPa)
Displacement normalized by gage length
HR Experiment
2354373: tauy0=2.0, m=0.3, e_f=140.6, e_t=
2354824: tauy0=2.0, m=0.3, e_f=140.6, e_t=
2354825: tauy0=2.0, m=0.3, e_f=140.6, e_t=
2355536: tauy0=2.0, m=0.3, e_f=140.6, e_t=
Traction-Separation Laws
Traction (MPa)
Displacement (mm)

Appendix B. Effect of the Poisson's Ratios and the Out-of-Plane Shear Modulus

The sub-mesoscale (SMS) approach modeled the unidirectional (UD) layer as transversely isotropic elastic. Therefore, there were five independent elastic constants: one independent shear modulus, the out-of-plane shear modulus G_{ft}, and two Poisson's ratios, ν_{ft} and ν_{tt}.

The effect of G_{ft} was demonstrated by rerunning the Set A IR simulation while changing only the value of this modulus. The following figure shows the simulated load-displacement response for three different values of G_{ft}.

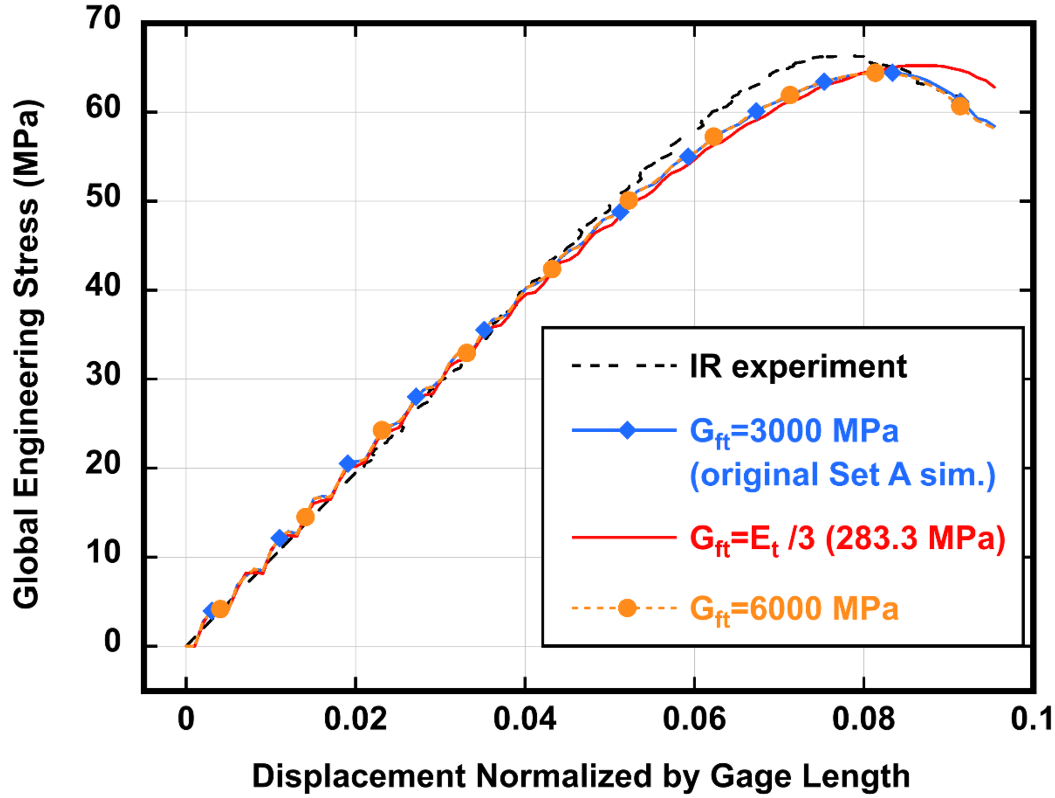

The effects of the Poisson's ratios were demonstrated by rerunning the Set A IR simulation while separately changing these ratios. The following figure shows the response. We note that changing ν_{tt} also affected the in-plane shear modulus, G_{tt}, due to the assumption of transverse isotropy:

$$G_{tt} = \frac{E_t}{2(1+\nu_{tt})}. \qquad \text{(B-1)}$$

The figure includes the calculated value of G_{tt} for ease of comparison.

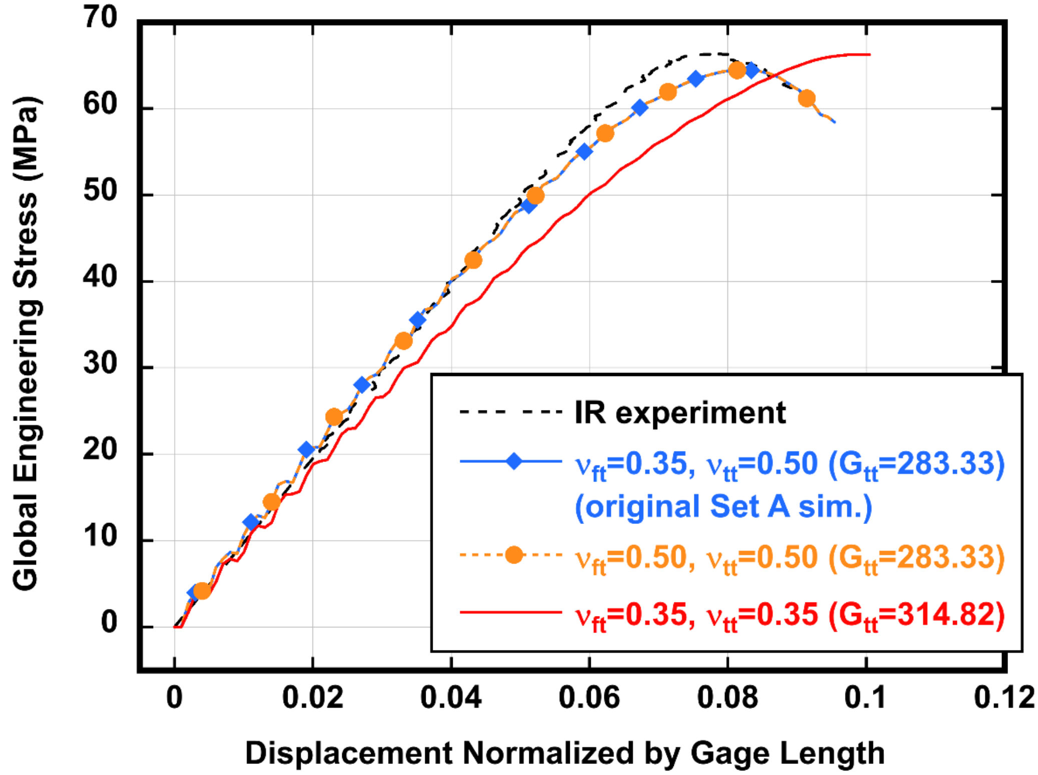

Global Engineering Stress (MPa)
70
60
50
40
30
20
10
0
0
0.02
0.04
0.06
0.08
0.1
0.12
Displacement Normalized by Gage Length
IR experiment
ν_{ft}=0.35, ν_{tt}=0.50 (G_{tt}=283.33)
(original Set A sim.)
ν_{ft}=0.50, ν_{tt}=0.50 (G_{tt}=283.33)
ν_{ft}=0.35, ν_{tt}=0.35 (G_{tt}=314.82)

Appendix C. Collection of Examples from Preliminary Simulations Using Prebuilt Options in LS-DYNA for Triangular and Trapezoidal Traction-Separation Laws (TSLs)

The Sets A–D simulations of fiber-based composites modeled delamination with a user-defined tiebreak model that featured a custom-shaped TSL. A custom-shaped TSL was used because load-displacement response from preliminary simulations using the prebuilt options in LS-DYNA[1] did not represent the experimental failure response. The options that were tried in the preliminary simulations included triangular-shaped TSLs, as in the previously documented film-based simulations, and also trapezoidal TSLs. This Appendix is a collection of examples from these preliminary simulations.

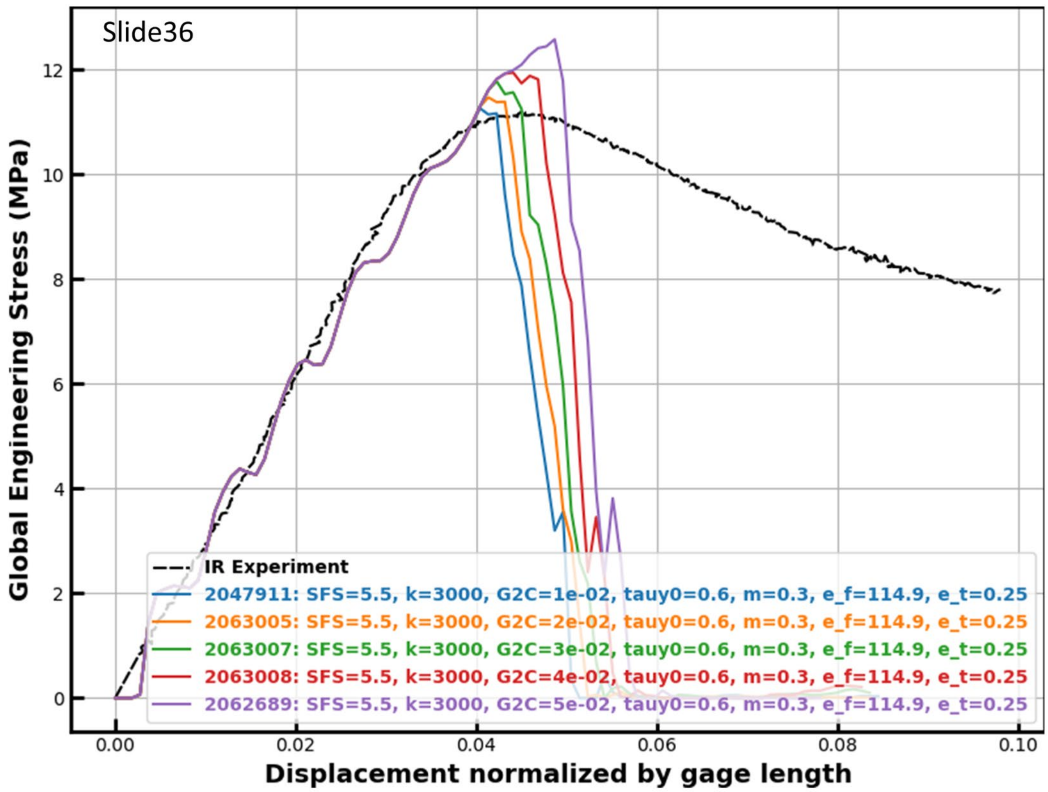

Fig. C-1 Effect of using triangular TSLs and maintaining the peak stress (SFS) and stiffness (k) constant while systematically increasing the total area under the curve (GIIC or shown in figure legend as "G2C")

The remaining figures follow the same format as in Appendix A: the load-displacement response is shown in the lefthand subfigure and the TSLs are shown in the inset subfigure on right. In the loading curves, the experimental loading response is shown with a black dotted line and the simulation responses with solid colored lines, with the color corresponding to the TSL. The examples do not follow a particular order, but are instead meant to be a repository where the interested

[1] LS-DYNA. LS-DYNA keyword user's manual volume I, II. Ver. R14.0. ANSYS; 2023 Feb 24.

reader seeking more detail can see the effects of the prebuilt options for TSLs in LS-DYNA by comparing outcomes.

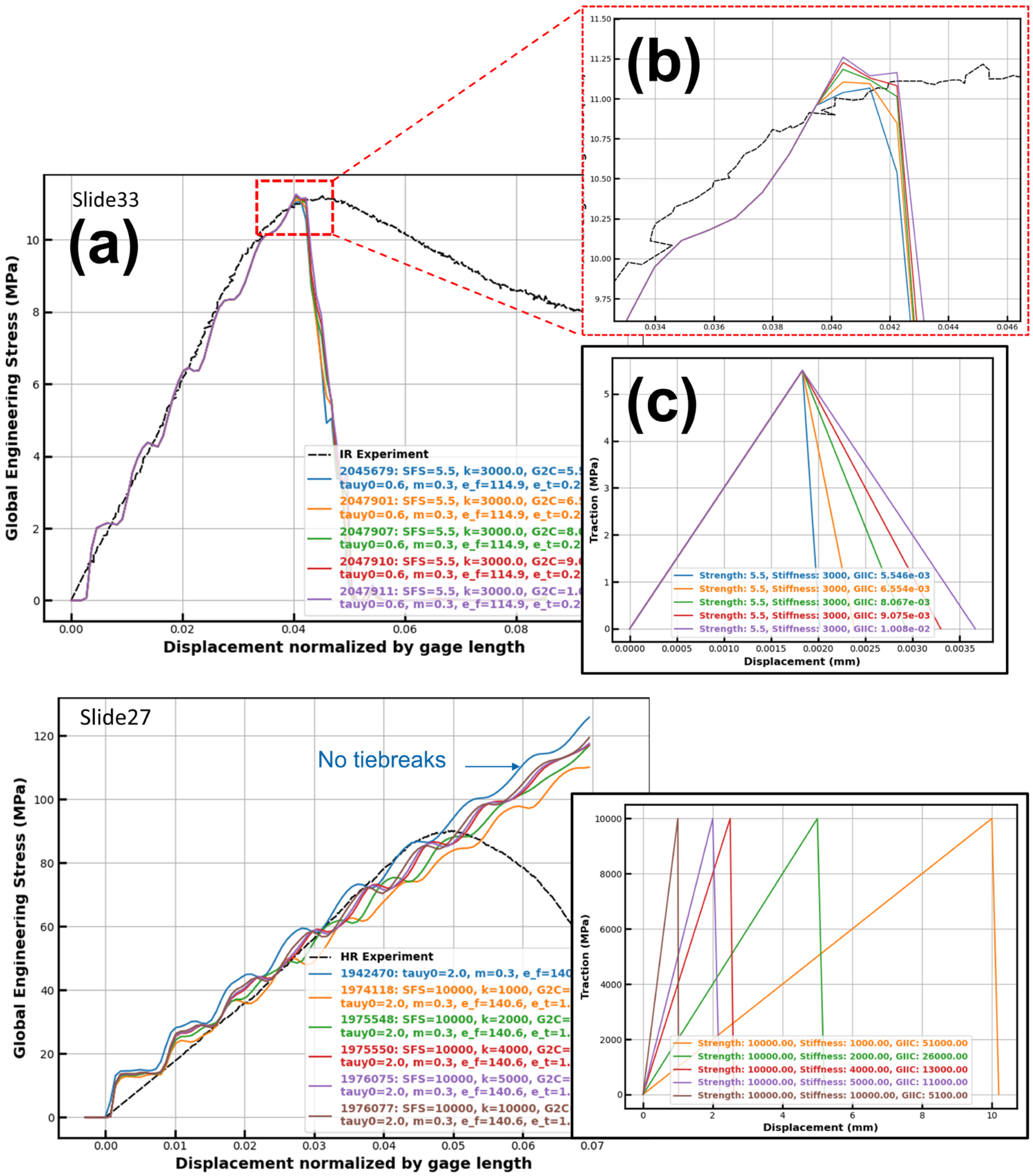

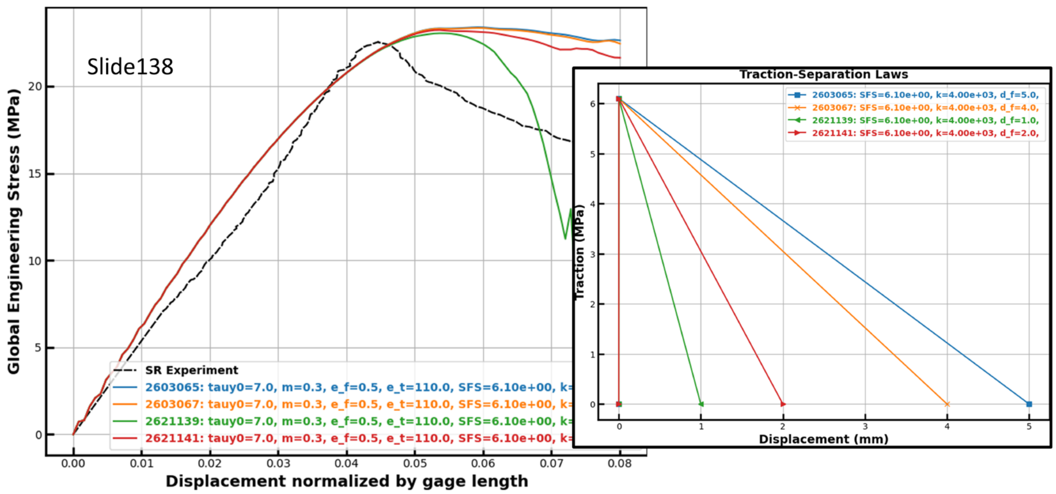
Slide138
Global Engineering Stress (MPa)
Displacement normalized by gage length
SR Experiment
2603065: tauy0=7.0, m=0.3, e_f=0.5, e_t=110.0, SFS=6.10e+00, k=
2603067: tauy0=7.0, m=0.3, e_f=0.5, e_t=110.0, SFS=6.10e+00, k=
2621139: tauy0=7.0, m=0.3, e_f=0.5, e_t=110.0, SFS=6.10e+00, k=
2621141: tauy0=7.0, m=0.3, e_f=0.5, e_t=110.0, SFS=6.10e+00, k=
Traction-Separation Laws
2603065: SFS=6.10e+00, k=4.00e+03, d_f=5.0,
2603067: SFS=6.10e+00, k=4.00e+03, d_f=4.0,
2621139: SFS=6.10e+00, k=4.00e+03, d_f=1.0,
2621141: SFS=6.10e+00, k=4.00e+03, d_f=2.0,
Traction (MPa)
Displacement (mm)

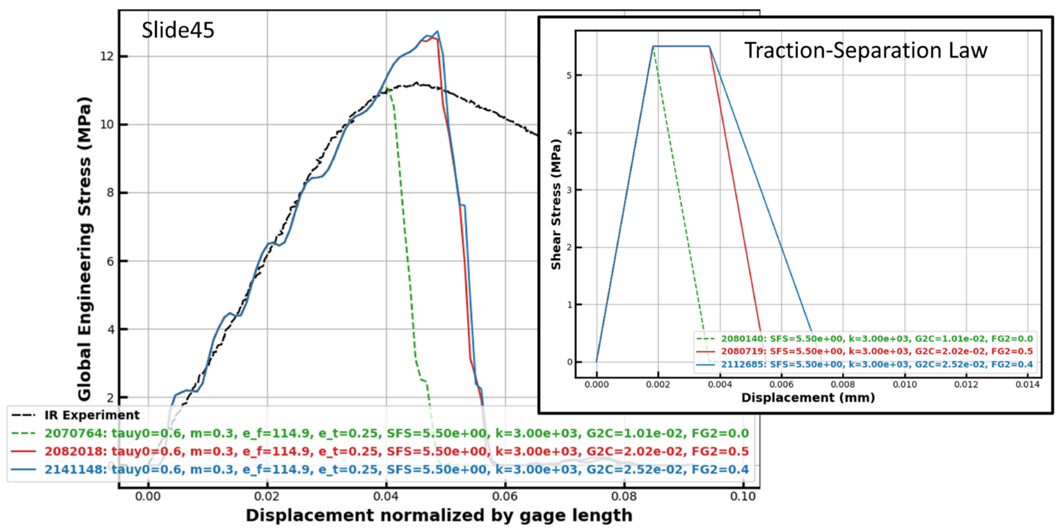
Slide45
Global Engineering Stress (MPa)
Displacement normalized by gage length
IR Experiment
2070764: tauy0=0.6, m=0.3, e_f=114.9, e_t=0.25, SFS=5.50e+00, k=3.00e+03, G2C=1.01e-02, FG2=0.0
2082018: tauy0=0.6, m=0.3, e_f=114.9, e_t=0.25, SFS=5.50e+00, k=3.00e+03, G2C=2.02e-02, FG2=0.5
2141148: tauy0=0.6, m=0.3, e_f=114.9, e_t=0.25, SFS=5.50e+00, k=3.00e+03, G2C=2.52e-02, FG2=0.4
Traction-Separation Law
Shear Stress (MPa)
Displacement (mm)
2080140: SFS=5.50e+00, k=3.00e+03, G2C=1.01e-02, FG2=0.0
2080719: SFS=5.50e+00, k=3.00e+03, G2C=2.02e-02, FG2=0.5
2112685: SFS=5.50e+00, k=3.00e+03, G2C=2.52e-02, FG2=0.4

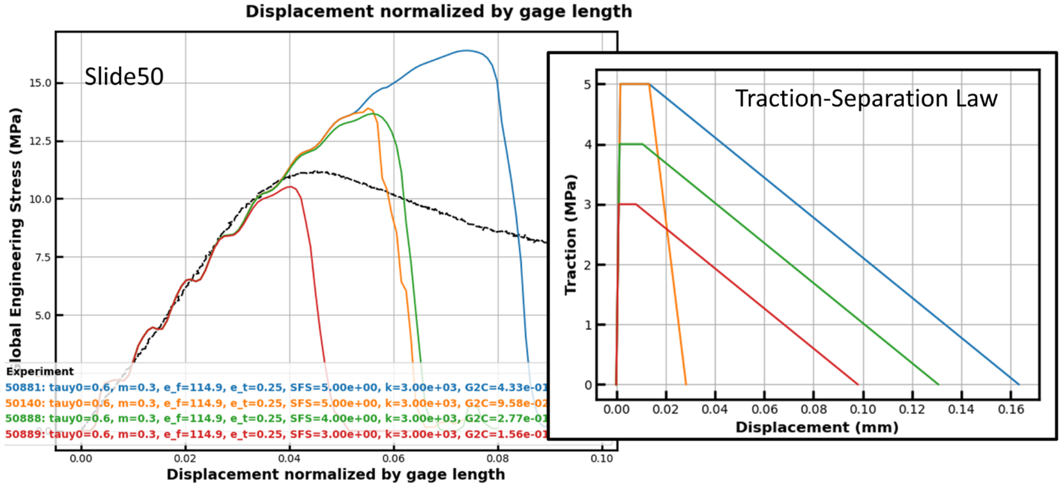
Slide50
lobal Engineering Stress (MPa)
Displacement normalized by gage length
Experiment
50881: tauy0=0.6, m=0.3, e_f=114.9, e_t=0.25, SFS=5.00e+00, k=3.00e+03, G2C=4.33e-01
50140: tauy0=0.6, m=0.3, e_f=114.9, e_t=0.25, SFS=5.00e+00, k=3.00e+03, G2C=9.58e-02
50888: tauy0=0.6, m=0.3, e_f=114.9, e_t=0.25, SFS=4.00e+00, k=3.00e+03, G2C=2.77e-01
50889: tauy0=0.6, m=0.3, e_f=114.9, e_t=0.25, SFS=3.00e+00, k=3.00e+03, G2C=1.56e-01
Traction-Separation Law
Traction (MPa)
Displacement (mm)

Appendix D. How to Set Up LS-DYNA Input File to Use the User-defined Tiebreak (UTB) Model with Custom-shaped Traction-Separation Law (TSL)

This Appendix provides instructions on how to set up the LS-DYNA[1] input file to use the UTB model we developed.

Preliminary notes:

- These instructions are for a single contact between two interacting parts. The methodology can be repeated for as many contacts as needed.
- These instructions use the high-rate values that were optimized for Set A. The values were documented previously in Table 3. User can interchange values as needed for other rates.
- The values shown here are based on the following unit system: length in millimeters, time in milliseconds, and mass in grams. This gives stress in Megapascals and force in Newtons. User will need to scale accordingly if using a different system of units.

Prerequisites:

- User needs a version of LS-DYNA[1] that is developed for implementing user-defined features. LS-DYNA refers to this as an "object version."
- UTB models are contained in the source file called `dyn21cnt.f`. This source file contains the subroutines titled `utb101` through `utb105`, which are meant to be placeholders for user-developed models. We chose to name the UTB that we developed here as `utb102`. User needs to replace the `utb102` placeholder in the `dyn21cnt.f` source file with our `utb102` routine and accompanying modules (available upon request from authors) and then recompile.

The UTB model requires the following additions to the input file:

- User needs to define segment sets on the two interacting sides via two *SET_SEGMENT cards.
- The TSLs in the shear and normal directions are defined with loading curves. We defined these via two *DEFINE_CURVE keywords. These are shown in Fig. D-1 and explained in the figure caption.
- Two contact keywords:
    - o `*CONTACT_AUTOMATIC_ONE_WAY_SURFACE_TO_SURFACE_TIEBREAK_USER`

[1] LS-DYNA. LS-DYNA keyword user's manual volume I, II. Ver. R14.0. ANSYS; 2023 Feb 24.

- *CONTACT_AUTOMATIC_SURFACE_TO_SURFACE
- Figure D-2 shows these two keywords. The parameters for these keywords are explained in Section D-1.

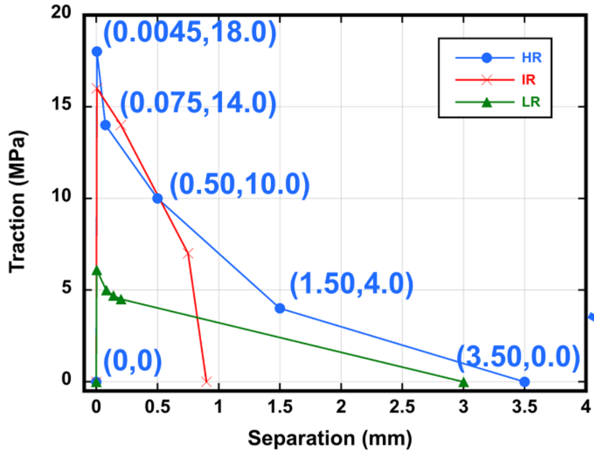


```
*DEFINE_CURVE_TITLE
TSL_SHEAR
$#    LCID      SIDR       SFA       SFO      OFFA      OFFO    DATTYP     LCINT
         2         0       1.0       1.0       0.0       0.0         0         0
$#                A1                  O1
                 0.0                 0.0
              0.0045               18.00
               0.075               14.00
                0.50               10.00
                1.50                4.00
                3.50                 0.0
               100.0                 0.0
*DEFINE_CURVE_TITLE
TSL_NORMAL
$#    LCID      SIDR       SFA       SFO      OFFA      OFFO    DATTYP     LCINT
         3         0       1.0       1.0       0.0       0.0         0         0
$#                A1                  O1
                 0.0                 0.0
                 1.0               1.0E5
                1.01                 0.0
               100.0                 0.0
```

Fig. D-1 The two curves used to define the TSLs. The first curve (LCID = 2) defines the TSL in the shear direction. The second curve (LCID = 3) defines the TSL in the normal direction. For each direction, the TSL is defined as a series of data points. The abscissa (under the A1 column) corresponds to the separation in mm, and the ordinate (under the O1 column) refers to the traction in MPa. The TSL is assumed to be formed by joining the data points with line segments. We set the TSL in the normal direction to an artificially high shape to essentially turn off delamination in the normal direction. For the shear direction, the data points listed under A1 and O1 refer to the coordinates defining the high-rate TSL reproduced in the top subfigure. All other parameters in these keywords have default values, and the reader is referred to LS-DYNA documentation for further explanation.

```
*CONTACT_AUTOMATIC_ONE_WAY_SURFACE_TO_SURFACE_TIEBREAK_USER
$#      CID                                                                 TITLE
$         1Title_for_Contact
$#    SURFA     SURFB  SURFATYP  SURFBTYP   SABOXID   SBBOXID      SAPR      SBPR
          1         2         0         0         0         0         0         0
$#       FS        FD        DC        VC       VDC    PENCHK        BT        DT
        0.0       0.0       0.0       0.0       0.0         0       0.01.00000E20
$#     SFSA      SFSB      SAST      SBST     SFSAT     SFSBT       FSF       VSF
        1.0       1.0       0.0       0.0       1.0       1.0       1.0       1.0
$#   OPTION       NHV     CT2CN        CN    OFFSET     NHMAT     NHWLD
        102         2      0.04     1.0E5         0         0         0
$#      UP1       UP2       UP3       UP4       UP5       UP6       UP7       UP8
       1.01      3.50       1.0     1.0E5      18.0    999999      -3.0      -2.0
$#      UP9      UP10      UP11      UP12      UP13      UP14      UP15      UP16
        0.0       0.0       0.0       0.0       0.0       0.0       0.0       0.0
*CONTACT_AUTOMATIC_SURFACE_TO_SURFACE
$#    SURFA     SURFB  SURFATYP  SURFBTYP   SABOXID   SBBOXID      SAPR      SBPR
          1         2         0         0         0         0         0         0
$#       FS        FD        DC        VC       VDC    PENCHK        BT        DT
        0.0       0.0       0.0       0.0       0.0         0       0.01.00000E20
$#     SFSA      SFSB      SAST      SBST     SFSAT     SFSBT       FSF       VSF
        1.0       1.0       0.0       0.0       1.0       1.0       1.0       1.0
```

Fig. D-2 The two contact keywords. Only the parameters that are highlighted in yellow have values different than the default LS-DYNA values. The highlighted non-default parameters are explained in Section D-1. The reader is referred to LS-DYNA documentation for explanation of all other parameters.

Explanation of Parameters in the Contact Keywords

- SURFA, SURFB: the identification numbers for the two interacting surfaces. The two surfaces are referred to as Surface A and Surface B. Surface A is treated as the "tracked" surface and Surface B as the "reference" surface, where the difference between the tracked and reference surfaces is explained in the LS-DYNA documentation and is outside the scope of the present report. We chose to define the interacting surfaces via segment sets (*SET_SEGMENT keyword) based on recommendation from LS-DYNA documentation. Therefore, SURFA and SURFB corresponded to the SIDs of the two *SET_SEGMENT keywords.

- SURFATYP, SURFBTYP: flags to indicate to LS-DYNA how Surface A and Surface B are defined. Since we defined the surfaces via segment sets, the corresponding code was 0.

- OPTION: indicates the subroutine that contains the UTB model. We chose to write our model as utb102, and therefore had to specify OPTION as 102.

- NHV: indicates number of history variables used in the UTB model. Our model uses two history variables.

- CN: stiffness (MPa/mm) of the TSL in the normal direction. We wanted the TSL in the normal direction to be essentially deactivated and so used a value of CN = 1.0e5 MPa for all rates.

- CT2CN: ratio between stiffness of the TSL in the shear direction (CT) to the stiffness of the TSL in the normal direction (CN) such that CT can be calculated as the product of CT2CN and CN. For high-rate, we specified a value of CT to be 4,000 MPa/mm (this can be seen in the TSL in Fig. D-1). Since CN was 1.0e5 for all rates, the CT2CN parameter was 0.04.
- UP1-UP8: user parameters that are passed to the UTB subroutine.
  - `UP1`: final separation (mm) at the end of the TSL in the normal direction. We used a value of 1.01 mm for all rates.
  - `UP2`: final separation (mm) at the end of the TSL in the shear direction. The high-rate value was 3.5 mm (see the TSL in Fig. D-1).
  - `UP3`: not currently used.
  - `UP4`: peak traction (MPa) of the TSL in the normal direction. We used a value of 1.0e5 MPa for all rates.
  - `UP5`: peak traction (MPa) of the TSL in the shear direction. We used a value of 18.0 for high-rate (see the TSL in Fig. D-1).
  - `UP6`: this is the node number of a node on Surface A. Our UTB only uses this to print out information to standard output that can be used for debugging and documentation purposes.
  - `UP7`: loading curve ID for the TSL in the normal direction. We set `UP7` = –3.0 because we had specified the `LCID` of the `*DEFINE_CURVE` keyword for the TSL in the normal direction to be `LCID` = 3 (see Fig. D-1). The negative value was used to indicate to LS-DYNA[1] to use exact representation of the loading curve rather than an approximation.
  - `UP8`: loading curve ID for the TSL in the shear direction. We set `UP7` = –3.0 because we had specified the `LCID` of the `*DEFINE_CURVE` keyword for the TSL in the normal direction to be `LCID`=3 (see Fig. D-1). The negative value was used to indicate to LS-DYNA to use exact representation of the loading curve rather than an approximation.

Appendix E. How to Set Up LS-DYNA Input File to use the Sub-Mesoscale (SMS) Material Model

E.1 Prerequisites and Preliminary Notes

The values shown here are based on the following unit system: length in millimeters, time in milliseconds, and mass in grams. This gives stress in Megapascals and force in Newtons. User will need to scale accordingly if using a different system of units.

User needs a version of LS-DYNA[1] that is developed for implementing user-defined features. LS-DYNA refers to this as an "object version."

The SMS material model was developed to be used as a vectorized user material (UMAT) model in LS-DYNA. In the object version of LS-DYNA, vectorized UMATs are located in the `dyn21umatv.f` source file. This file contains various subroutines including `UMAT41V`, `UMAT42V`, and so forth, through `UMAT50V`. We have chosen to develop the SMS material model using the title `UMAT42V`. Therefore, the user must replace the default `UMAT42V` subroutine in the `dyn21umatv.f` source file with the SMS material model and its accompanying modules and subroutines, which are available from the authors.

E.2 Setting Up the LS-DYNA Input File

The SMS material model can be assigned to a part by the `*MAT_USER_DEFINED_MATERIAL_MODELS` keyword, referred to here in shortened form as `*MAT_USER`. The keyword consists of five total lines, which are referred to in LS-DYNA as data cards.

The first two data cards specify various flags used for LS-DYNA.

The third and subsequent data cards list the material properties used by the material model. We have chosen to set up our simulations by listing the material properties in the global coordinate system. Therefore, we used two different `*MAT_USER` keywords:

- One keyword was for the 0° unidirectional (UD) layer, defined such that fibers were in the global 1-direction and the global 2- and 3-directions were isotropic. Figure E-1 (top) shows how to set up the keyword for this layer.
- Another keyword was for the 90° UD layer defined such that fibers were in the global 2-direction and the global 1- and 3-directions were isotropic. Figure E-1 (bottom) shows how to set up the keyword for this layer.

[1] LS-DYNA. LS-DYNA keyword user's manual volume I, II. Ver. R14.0. ANSYS; 2023 Feb 24.

The differences between the keywords for the 0° and 90° layers were almost exclusively in the third through fifth data cards listing the material properties. The first two data cards were essentially the same for the two different layers. The sole exception was for MID, which is the identification number and must be unique for each material.

We chose to specify the data for many of the fields in the *MAT_USER keywords using variables that we defined in our input file through *PARAMETER and *PARAMETER_EXPRESSION keywords. Figure E-2 shows how to write these two keywords using the high-rate values from the Set A simulations. As shown in Fig. E-1, the variables are referenced in the *MAT_USER keywords by prepending the actual variable name with an ampersand symbol (&). The variables are originally defined in the parameter keywords by prepending the variable name with the letter "R", which indicates that the variables are stored as real numbers.

```
*MAT_USER_DEFINED_MATERIAL_MODELS_TITLE
SMS_HB25_0_LAYER
$#     MID        RO        MT       LMC       NHV    IORTHO     IBULK        IG
         1  9.940E-4        42        22        64         0         1         2
$#   IVECT     IFAIL    ITHERM    IHYPER      IEOS      LMCA    UNUSED    UNUSED
         1         1         0         1         0         0
$#      P1        P2        P3        P4        P5        P6        P7        P8
   &DYNA_K   &DYNA_G      &E_F      &E_T      &E_T    &NU_FT    &NU_TT     &G_FT
$#      P9       P10       P11       P12       P13       P14       P15       P16
    &NU_FT     &G_FT     &G_TT       0.0&GAM_0_DOT    &TAU_Y        &M       6.0
$#     P17       P18       P19       P20       P21       P22       P23       P24
       1.0       0.0      15.0       0.0    1200.0     500.0       0.0       0.0
*MAT_USER_DEFINED_MATERIAL_MODELS_TITLE
SMS_HB25_90_LAYER
$#     MID        RO        MT       LMC       NHV    IORTHO     IBULK        IG
         2  9.940E-4        42        22        64         0         1         2
$#   IVECT     IFAIL    ITHERM    IHYPER      IEOS      LMCA    UNUSED    UNUSED
         1         1         0         1         0         0
$#      P1        P2        P3        P4        P5        P6        P7        P8
   &DYNA_K   &DYNA_G      &E_T      &E_F      &E_T    &NU_TF    &NU_FT     &G_FT
$#      P9       P10       P11       P12       P13       P14       P15       P16
    &NU_TT     &G_TT     &G_FT       0.0&GAM_0_DOT    &TAU_Y        &M       6.0
$#     P17       P18       P19       P20       P21       P22       P23       P24
       0.0       0.0      15.0         0    1200.0     500.0         0         0
```

Fig. E-1 The material keywords for a 0° layer (top) and 90° layer (bottom). First two data cards (lines) are flags used by LS-DYNA and are described in Section E.2.1. The remaining data cards are for P1-P22, which are the material properties used in the SMS model and are described in Section E.2.2. We chose to provide the data for many of the fields via variables. The variables are included in the data cards here by prepending with the ampersand (&) symbol (e.g., the variable TAU_Y is written for P14 as "&TAU_Y"). Figure E-2 shows how to specify the variables in the input deck with the high-rate values.

```
*PARAMETER
$Elastic Parameters
RE_F      110000.0
RE_T      1500.0
RNU_FT    0.35
RNU_TT    0.50
RG_FT     3000.0
$Crystal plasticity parameters
RTAU_Y    18.0
RM        0.15
RGAM_0_DOT, 1.0e-3
$Bulk and shear modulus to send to LS-DYNA
RDYNA_K   115000.0
RDYNA_G   3000.0
*PARAMETER_EXPRESSION
RG_TT,  E_T/(2.0*(1.0+NU_TT))
RNU_TF, NU_FT*(E_T/E_F)
```

Fig. E-2 The two keywords that define the variables used by the material keyword in Fig. E-1 with the values from the high-rate Set A values. Here, all variable names are prepended with the letter "R" (e.g., the variable TAU_Y is listed as "RTAU_Y").

E.2.1 First Two Data Cards of Material Keywords

The following is a simplified explanation of the flags in the first two data cards. These explanations are copied in shortened form from Alexander et al.,[2] where we provided more details. Reader is referred to Alexander et al.[2] and LS-DYNA[1] documentation for further details.

- `MID`: material identification number. User must choose an integer number distinct from any other material used in the simulation.
- RO: mass density (g/mm^3) of the ultra-high-molecular-weight polyethylene (UHMWPE). For HB25, we use 9.94e-4 g/mm^3 from the measurements reported in Alexander and Weerasooriya.[3]
- MT: must be set to 42 to match the title of the subroutine for our SMS model, which has the title UMAT42V.
- LMC and LMCA: refers to the number of material parameters listed on the third and subsequent data cards. Must be set to `LMC`=22 and `LMCA`=0 for the SMS model.

---

[2] Alexander SL, Becker R, Weerasooriya T. User guide to a wrapper that allows a custom user-defined material model (UMAT) originally developed for Abaqus/EPIC to be used in LS-DYNA simulations. DEVCOM Army Research Laboratory (US); 2023a Oct. Report No.: ARL-TN-1177. https://apps.dtic.mil/sti/trecms/pdf/AD1214015.pdf

[3] Alexander SL, Weerasooriya T. Mechanical characterization of advanced ultra-high molecular weight polyethylene (UHMWPE) composites by ultrasonic method. DEVCOM Army Research Laboratory (US); 2021 Aug. Report No.: ARL-TR-9254. https://apps.dtic.mil/sti/pdfs/AD1146645.pdf

- NHV: refers to the number of history variables. Must be set to 64 for the SMS model used here.
- IORTHO: must be set to 0.
- IBULK and IG: these indicate the position within the material properties (third and subsequent data cards) of estimates for the bulk and shear modulus of the material that are required to be supplied to LS-DYNA. We set IBULK = 1 and IG = 2 because we supplied estimates for the bulk modulus as P1 and the shear modulus as P2 (see Table E-1).
- IVECT: must be set to 1 to indicate to LS-DYNA that our wrapper is a vectorized user material model rather than a serial material model.
- IFAIL: is a flag to indicate whether the material model intends to delete elements that meet a failure criterion. We set this to 1. The current version of SMS model does not account for other failure modes except delamination, but in future we intend to add other modes of failure to this as an extension.
- ITHERM: we have been using ITHERM = 0 because the SMS model does not handle any temperature variables.
- IHYPER: must be set to 1 in order for LS-DYNA[1] to send the deformation gradient to the SMS model.
- IEOS: is for equation of state. We have been using IEOS=0.

E.2.2 Third, Fourth, and Fifth Data Cards of the Material Keywords

User needs to specify a total of 22 parameters, which are listed on the material keyword as P1 through P22. There are eight parameters per data card. The remaining parameters on the fifth data card (P23 and P24) are left with default value of 0 since they are unused. Table E-1 describes the parameters P1 through P22 for a 0° UD layer, defined by having fibers arranged in the global 1-direction. Table E-2 is for a 90° UD layer, defined by having fibers arranged in the global 2-direction.

Table E-1 Material parameters used by the material keyword for running the SMS model for a 0° layer (when fibers are oriented in the global 1-direction)

Param. No. in LS-DYNA	Description	Sym. for 0° UD layer	Units	Values for 0° UD layer		
				LR	IR	HR
P1	Estimated bulk modulus for LS-DYNA	~	MPa	1.103e5	1.105e5	1.150e5
P2	Estimated shear modulus for LS-DYNA	~	MPa	3.0e3	3.0e3	3.0e3
P3	Young's modulus in 1-direction	E_f	MPa	1.1e5	1.1e5	1.1e5
P4	Young's modulus in 2-direction	E_t	MPa	500.0	850.0	1500.0
P5	Young's modulus in 3-direction	E_t	MPa	500.0	850.0	1500.0
P6	Poisson's ratio in 1-2 direction	ν_{ft}	[none]	0.35	0.35	0.35
P7	Poisson's ratio in 2-3 direction	ν_{tt}	[none]	0.50	0.50	0.50
P8	Shear modulus in 1-2 direction	G_{ft}	MPa	3000.0	3000.0	3000.0
P9	Poisson's ratio in 1-3 direction	ν_{ft}	[none]	0.35	0.35	0.35
P10	Shear modulus in 3-1 direction	G_{ft}	MPa	3000.0	3000.0	3000.0
P11	Shear modulus in 2-3 direction	G_{tt}	MPa	166.67	283.33	500.00
P12	(currently unused)	~	~	0	0	0
P13	Reference shear strain rate	$\dot{\gamma}_0$	ms^{-1}	100.000	0.400	0.001
P14	Reference shear yield strength of UD layer	τ_y^0	MPa	18.0	18.0	18.0
P15	Rate sensitivity exponent	m	[none]	0.15	0.15	0.15
P16	Number of slip systems	~	integer	6	6	6
P17	Flag indicating 0° or 90° UD layer	~	integer	1	1	1
P18	Angle of rotation about 3-direction	~	degrees	User must specify angles based on configuration of UHMWPE		
P19	Angle of rotation about 2-direction	~	degrees			
P20	Angle of rotation about 1-direction	~	degrees			
P21	Tensile failure threshold (not actively used in current version but must be set to a value greater than 0)	~	MPa	1200.0	1200.0	1200.0
P22	Shear failure threshold (not actively used in current version but must be set to a value greater than 0)	~	MPa	500.0	500.0	500.0

Table E-2 Material parameters used by the material keyword for running the SMS model for a 90° layer (when fibers are oriented in the global 2-direction)

Param. No. in LS-DYNA	Description	Sym. for 90° UD layer	Units	Values for 90° UD layer		
				LR	IR	HR
P1	Estimated bulk modulus for LS-DYNA	~	MPa	1.103e5	1.105e5	1.150e5
P2	Estimated shear modulus for LS-DYNA	~	MPa	3.0e3	3.0e3	3.0e3
P3	Young's modulus in 1-direction	E_t	MPa	500.0	850.0	1500.0
P4	Young's modulus in 2-direction	E_f	MPa	1.1e5	1.1e5	1.1e5
P5	Young's modulus in 3-direction	E_t	MPa	500.0	850.0	1500.0
P6	Poisson's ratio in 1-2 direction	ν_{tf}	[none]	0.00159	0.00270	0.00477
P7	Poisson's ratio in 2-3 direction	ν_{ft}	[none]	0.35	0.35	0.35
P8	Shear modulus in 1-2 direction	G_{ft}	MPa	3000.0	3000.0	3000.0
P9	Poisson's ratio in 1-3 direction	ν_{tt}	[none]	0.50	0.50	0.50
P10	Shear modulus in 3-1 direction	G_{tt}	MPa	166.67	283.33	500.0
P11	Shear modulus in 2-3 direction	G_{ft}	MPa	3000.0	3000.0	3000.0
P12	(currently unused)	~	~	0	0	0
P13	Reference shear strain rate	$\dot{\gamma}_0$	ms^{-1}	100.000	0.400	0.001
P14	Reference shear yield strength of UD layer	τ_y^0	MPa	18.0	18.0	18.0
P15	Rate sensitivity exponent	m	[none]	0.15	0.15	0.15
P16	Number of slip systems	~	integer	6	6	6
P17	Flag indicating 0° or 90° UD layer	~	integer	0	0	0
P18	Angle of rotation about 3-direction	~	degrees	User must specify angles based on configuration of UHMWPE		
P19	Angle of rotation about 2-direction	~	degrees			
P20	Angle of rotation about 1-direction	~	degrees			
P21	Tensile failure threshold (not actively used in current version but must be set to a value greater than 0)	~	MPa	1200.0	1200.0	1200.0
P22	Shear failure threshold (not actively used in current version but must be set to a value greater than 0)	~	MPa	500.0	500.0	500.0

Appendix F. How to Set Up LS-DYNA to Use the Elemental Macroscale (EMS) Material Model

F.1 Prerequisites and Preliminary Notes

The values shown here are based on the following unit system: length in millimeters, time in milliseconds, and mass in grams. This gives stress in Megapascals and force in Newtons. User will need to scale accordingly if using a different system of units.

User needs a version of LS-DYNA that is developed for implementing user-defined features. LS-DYNA[1] refers to this as an "object version."

The EMS material model was originally developed for Abaqus/EPIC finite element programs. Therefore, a wrapper is required in order to use the EMS material model in LS-DYNA.[1] We previously documented and described a wrapper we developed for this purpose. The present instructions assume that the user is using our wrapper.

Reader is referred to Alexander et al.[2] for a complete description of the wrapper. Briefly, the wrapper is a LS-DYNA user-defined material (UMAT) subroutine that acts as an interface between the LS-DYNA program and the Abaqus/EPIC model. The title of the UMAT is `UMAT42V`. The present instructions assume that the user has followed the steps described in Section 3.2 of Alexander et al. "Compile LS-DYNA to Use the Wrapper."[2]

F.2 Setting Up the LS-DYNA Input File

The EMS material model can be assigned to a part via the `*MAT_USER_DEFINED_MATERIAL_MODELS` keyword. Figure F-1 shows how to write this keyword.

- The first two lines (referred to as data cards in LS-DYNA) consist of flags used by LS-DYNA. Section F.2.1 explains these data cards.
- The third and subsequent data cards consist of the parameters that are used by the wrapper in order to run the EMS material model. Section F.2.2 explains these data cards.

We chose to specify the data for many of the fields in the material keyword using variables that we defined in our input file through `*PARAMETER` and `*PARAMETER_EXPRESSION` keywords. Figure F-2 shows how to write these two keywords using the high-rate values from the re-optimized simulations (Set D).

[1] LS-DYNA. LS-DYNA keyword user's manual volume I, II. Ver. R14.0. ANSYS; 2023 Feb 24.
[2] Alexander SL, Becker R, Weerasooriya T. User guide to a wrapper that allows a custom user-defined material model (UMAT) originally developed for Abaqus/EPIC to be used in LS-DYNA simulations. DEVCOM Army Research Laboratory (US); 2023a Oct. Report No.: ARL-TN-1177. https://apps.dtic.mil/sti/trecms/pdf/AD1214015.pdf

As shown in Fig. F-1, the variables are referenced in the material keyword by prepending the actual variable name with an ampersand symbol (&). The variables are originally defined in the parameter keywords by prepending the variable name with the letter "R", which indicates that the variables are stored as real numbers.

```
*MAT_USER_DEFINED_MATERIAL_MODELS_TITLE
EMS_HB25
$#     MID        RO        MT       LMC       NHV    IORTHO     IBULK        IG
         1      &RHO        42        34        33         0         1         2
$#   IVECT     IFAIL    ITHERM    IHYPER      IEOS      LMCA    UNUSED    UNUSED
         1         0         0         1         0         0
$#      P1        P2        P3        P4        P5        P6        P7        P8
   &DYNA_K   &DYNA_G        24        30      &RHO      &XMU     &BULK    &BULKP
$#      P9       P10       P11       P12       P13       P14       P15       P16
   &YLDMAT   &MCONST     &MEXP    &MNORM   &YLDSLP   &RCONST     &REXP    &RNORM
$#     P17       P18       P19       P20       P21       P22       P23       P24
    &MVISC   &MVSCAP     &FMOD    &FFAIL    &FSOFT   &DEGRAD   &FFPOFF   &FVFRAC
$#     P25       P26       P27       P28       P29       P30       P31       P32
   &IMPLIC   &NF_FAM         0         0         1         1         0         0
$#     P33       P34       P35       P36       P37       P38       P39       P40
         0        90         0         0         0         0         0         0
```

Fig. F-1 The material keyword. Any entry prepended with the ampersand (&) symbol (e.g., &RHO) is a variable that must be defined using the parameter keywords shown in Fig. F-2.

```
*PARAMETER
$EMS PARAMETERS
RRHO,        9.94e-4
RBULKP,      8.0
RYLDMAT,     50.0
RMCONST,     0.0
RMEXP        0.35
RMNORM,      1.0e-3
RYLDSLP,     2.200
RRCONST,     2.0e5
RREXP,        0.15
RMVISC,      0.0
RMVSCAP,     -1.0
RFMOD,       110000.0
RFFAIL,      4.0e3
RFSOFT,      0.1
RDEGRAD,     1.2
RFFPOFF,     0.0
RFVFRAC,     0.95
RIMPLIC,     0.0
RNF_FAM,     2.0
$Parameters from SMS
RE_T       1500.0
RNU_FT     0.35
RNU_TT     0.50
*PARAMETER_EXPRESSION
$EMS Parameters
RXMU,        E_T/(2.0*(1.0+NU_TT))
RBULK,       1250.0
RRNORM,      1.0e-3
$For LS-DYNA:
RDYNA_K,     5.0*BULK
RDYNA_G,     5.0*XMU
```

Fig. F-2 The two keywords that define the variables used by the material keyword in Fig. F-1 with the values from the high-rate Set D (re-optimized) values. Here, all variable names are prepended with the letter "R" (e.g., the variable RHO is listed as RRHO).

F.2.1 First Two Data Cards of Material Keyword

The first two data cards have been explained in Alexander et al.[2] For convenience, the explanations are reproduced in shortened form as follows. Reader is referred to Alexander et al.[2] and LS-DYNA[1] documentation for more detail.

- `MID`: material identification number. User must choose an integer number distinct from any other material used in the simulation.
- RO: mass density (g/mm^3) of the ultra-high-molecular-weight polyethylene (UHMWPE). For HB25, we use 9.94e-4 g/mm^3 from the measurements reported in Alexander and Weerasooriya.[3]
- MT: must be set to 42 to match the title of the subroutine in the wrapper, which has the title UMAT42V.
- LMC and LMCA: refers to the number of material parameters listed on the third and subsequent data cards. Must be set to LMC = 34 and LMCA = 0. Appendix D of Alexander et al.[2] provides more details.
- NHV: refers to the number of history variables. Must be set to 33 for the wrapper. Appendix E in Alexander et al.[2] provides more information regarding the history variables.
- IORTHO: must be set to 0.
- IBULK and IG: these indicate the position within the material properties (third and subsequent data cards) of estimates for the bulk and shear modulus of the material that are required to be supplied to LS-DYNA. We set IBULK = 1 and IG = 2 because we supplied estimates for the bulk modulus as P1 and the shear modulus as P2 (see Table F-1).
- IVECT: must be set to 1 to indicate to LS-DYNA that our wrapper is a vectorized user material model rather than a serial material model.
- IFAIL: is a flag to indicate whether the material model intends to delete elements that meet a failure criterion. Should be set to 0 because the wrapper does not fail elements.
- ITHERM: we have been using `ITHERM` = 0 because the wrapper does not handle any temperature variables.

[3] Alexander SL, Weerasooriya T. Mechanical characterization of advanced ultra-high molecular weight polyethylene (UHMWPE) composites by ultrasonic method. DEVCOM Army Research Laboratory (US); 2021 Aug. Report No.: ARL-TR-9254. https://apps.dtic.mil/sti/pdfs/AD1146645.pdf

- `IHYPER`: must be set to 1 in order for LS-DYNA[1] to send the deformation gradient to the wrapper, which is needed by the EMS model (Appendix E in Alexander et al.[2]).
- IEOS: is for equation of state. We have been using `IEOS` = 0.

F.2.2 Third and Subsequent Data Cards of Material Keyword, Which List the Material Parameters

User needs to specify a total of 34 parameters, which are listed on the material keyword as P1 through P34. There are eight parameters listed per data card. The remaining parameters on the final data card (P35 through P40) are left with a default value of 0 since they are unused. Table F-1 describes the parameters P1 through P34.

The EMS model accounts for families of fibers. All fiber families are modeled as being in the same plane. The initial configuration of the fiber plane is defined by the unit vector of the direction of the first fiber family, M0, and the unit vector in the normal direction of the plane, NORM0. User must specify the three components of each of these two vectors in parameters P27 through P32. Figure F-3 provides an example of how to determine NORM0 and M0. User must verify application to their specific loading configuration.

Table F-1 Material parameters used by the material keyword for running the EMS material model by means of the wrapper

Param. no. in LS-DYNA	Description	Sym. in Table 4	Units	Values		
				LR	IR	HR
P1	Estimated bulk modulus for LS-DYNA	~	MPa	2085	3540	6250
P2	Estimated shear modulus for LS-DYNA	~	MPa	833.33	1416.67	2500.00
P3	No. of state vars. used in the EMS model	~	integer	24	24	24
P4	No. of material props. used in EMS model	~	integer	30	30	30
P5	Material density	ρ	kg/m^3	9.94e-4	9.94e-4	9.94e-4
P6	Matrix shear modulus	μ	MPa	166.67	283.33	500
P7	Matrix bulk modulus	κ	MPa	417	708	1250
P8	Pressure derivative of κ	κ'	[none]	8	8	8
P9	Von Mises yield strength of matrix	~	MPa	50	50	50
P10	Matrix rate sensitivity constant	~	[none]	0	0	0
P11	Matrix rate sensitivity exponent	~	[none]	0.35	0.35	0.35
P12	Normalization for matrix strain rate dependence	~	[none]	0.001	0.001	0.001
P13	Slip strength in fiber plane	$\hat{\tau}_0$	MPa	2.200	2.200	2.200
P14	Coefficient for log term in slip strength	$\hat{c}$	[none]	2×10^5	2×10^5	2×10^5
P15	Exponent for strain rate in slip strength	$\hat{m}$	[none]	0.15	0.15	0.15
P16	Reference slip rate	$\dot{\hat{\gamma}}_0$	ms^{-1}	100.000	0.400	0.001
P17	Matrix viscosity (not used)	~	~	0	0	0
P18	Matrix viscosity stress cap (not used)	~	~	–1	–1	–1
P19	Elastic modulus for single fiber	E	MPa	110,000	110,000	110,000
P20	Failure stress for single fiber/film	σ_{ff}	MPa	4000	4000	4000
P21	Fiber softening factor	~	[none]	0.1	0.1	0.1
P22	Fiber degradation for progressive failure after peak stress	~	[none]	1.2	1.2	1.2
P23	Fiber failure pressure offset	~	[none]	0	0	0
P24	Fiber volume fraction	~	fraction	0.95	0.95	0.95
P25	Flag to turn on modulus calculation	~	integer	0	0	0
P26	Number of fiber families	~	integer	2	2	2
P27	First component of NORM0 unit vector	~	[none]	NORM0 and M0 vectors depend on configuration of UHMWPE in simulation (example provided in Fig. F-3)		
P28	Second component of NORM0 unit vector	~	[none]			
P29	Third component of NORM0 unit vector	~	[none]			
P30	First component of M0 unit vector	~	[none]			
P31	Second component of M0 unit vector	~	[none]			
P32	Third component of M0 unit vector	~	[none]			
P33	Angle of first fiber family in the plane defined by NORM0 and M0	~	degrees	0	0	0
P34	Angle of second fiber family in the plane defined by NORM0 and M0	~	degrees	90	90	90

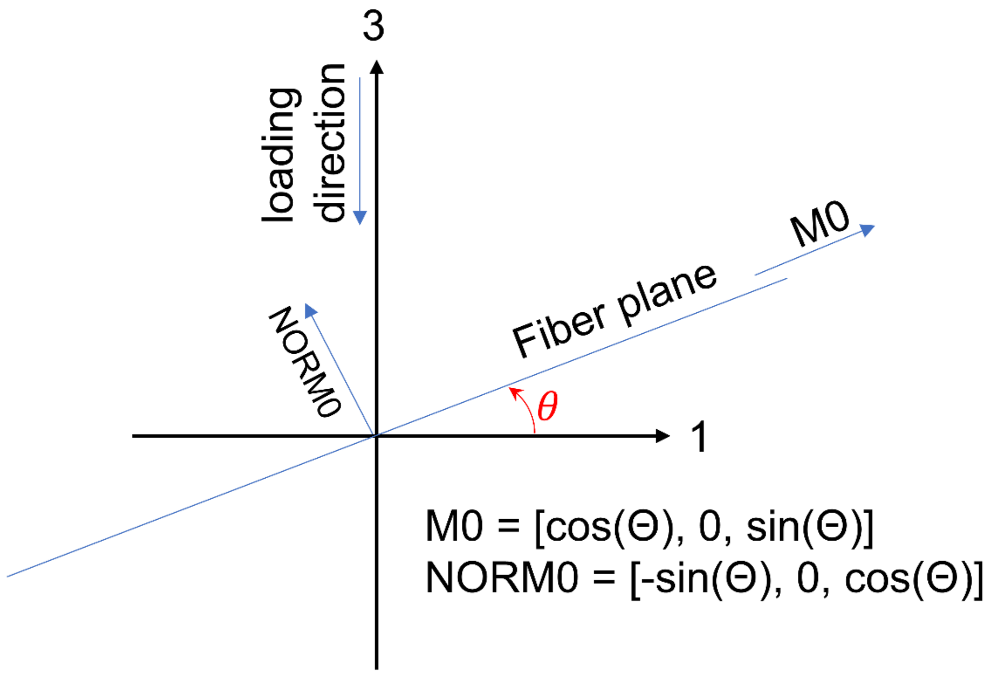

Fig. F-3 Example of how to calculate the M0 and NORM0 vectors, which define the plane of the UHMWPE in the EMS model in the initial configuration. This example assumes that the UHMWPE plane is rotated only about the global 2-direction. User will need to modify for other configurations.

List of Symbols, Abbreviations, and Acronyms

EMS	elemental macroscale
DOD	Department of Defense
FE	finite element
HPC	High Performance Computing
HR	high rate
IR	intermediate rate
LR	low rate
OALS	off-axis loaded shear
SF	scaling factor
SFS	Shear Failure Stress
SMS	sub-mesoscale
SSE	solid state extrusion
TSL	traction-separation law
UD	unidirectional
UHMWPE	ultra-high-molecular-weight polyethylene
UMAT	user material
UTB	user-defined tiebreak